DISTINGUISHING ALLOSTERIC INTERACTIONS USING THERMODYNAMIC ANALYSIS AND THE FIRST REPORTED CRYSTAL STRUCTURE OF PHOSPHO(ENOL)PYRUVATE BOUND E. COLI PHOSPHOFRUCTOKINASE

A Dissertation

by

BOBBY WAYNE LAIRD

Submitted to the Office of Graduate and Professional Studies of
Texas A&M University
in partial fulfillment of the requirements for the degree of

DOCTOR OF PHILOSOPHY

Chair of Committee,	Gregory D. Reinhart
Committee Members,	Mary Bryk
	Timothy Devarrene
	Paul Lindahl
Head of Department,	Gregory D. Reinhart

May 2015

Major Subject: Biochemistry

ABSTRACT

To better understand the relationship between allosteric ligand structure and the resulting allosteric behavior, we investigated the roles that functional groups and structure play in the binding affinity and allosteric potency of ligands at the allosteric site of phosphofructokinase from E. coli (EcPFK). EcPFK is allosterically inhibited and activated in the presence of phospho-enol-pyruvate (PEP) and MgADP, respectively. Both activator and inhibitor bind to the same effector site and result in modification of the affinity for the substrate fructose-6-phosphate (F6P). The fact that both MgADP and PEP bind to the same binding site using a majority of the same residues, makes EcPFK an ideal system for this type of allosteric characterization.

In order to better understand the structural affects that PEP has on EcPFK, here we present the first study of the crystal structure of EcPFK that has been solved with PEP bound to the allosteric binding sites (EcPEP). The disproportionation reaction, EA + XE ↔ E + XEA, describes the equilibrium between the two binary complexes, i.e. the enzyme bound to substrate (EA) or allosteric effector (XE), on one side of the equilibrium and on the other side is the apo enzyme (E) and the ternary complex (XEA), i.e. where both substrate and allosteric ligand are bound. When accounting for the disproportionation equilibrium, the known crystal structures of EcPFK can be identified as a specific species and characterized independently of the other species. Given the disproportionation reaction, EcPEP is the only known crystal structure of an EcPFK binary complex. EcATC represents the ternary complex while EcApo represents the unbound enzyme.

To specifically address the roles of allosteric ligand functional groups, thermodynamic linkage analysis was used to examine wild type EcPFK in the presence of allosteric ligand analogs. This analysis allowed for a particular effector ligand functional group to be assigned as important to ligand binding, to allosteric coupling, to both binding and coupling, or to neither binding nor coupling. As a complement to the allosteric ligand analog study, we used thermodynamic linkage analysis to study EcPFK with mutations in the allosteric binding site. Specifically, position 58 was examined and compared to the allosteric ligand analog results.

DEDICATION

This work is dedicated to Jenny, Mom (Annie), Dad (Ken), Kristine, Rusty, Roger, Lisa, Lina, Chris, Laura, Tim, their children, and their grandchildren. Thank you for each of the roles you have played in my journey to reach this point. Your time, love, conversations, and prayers were greatly appreciated.

ACKNOWLEDGEMENTS

I would like to thank my committee chair, Dr. Reinhart, and my committee members, Dr. Bryk, Dr. Devarenne, and Dr. Lindahl, for their guidance and support throughout my tenure at Texas A&M. I would also like to thank all of the Reinhart lab members, past and present, for their help and discussions over the years. I would especially like to thank Dr. Lasagna of the Reinhart lab for his guidance and influence over the years. Thank you to Jennifer Tsai of the Sacchettinni lab for help with crystallization, and to the Raushel lab for organic synthesis.

Thanks also go out to my friends and colleagues and the Bio/Bio faculty and staff for making my time at Texas A&M University such a special place to be. A very special thanks to Robert, Drew, and Texas A&M Football.

Finally, thanks to my mother and father for their encouragement and never ending encouragement. Thanks to my family: Kristine, Rusty, Daniel, Tiffany, Roger, Lisa, Becka, Brendan, Lina, Chris, Graham, Baby, Laura, Tim, Kayleigh, Kade, and all the grandchildren I failed to list. Especially thank you to Roger, Graham, Tim, and Chris for all of the distractions that you provided. Most of all I want to say thank you to my beautiful and intelligent wife for her patience, guidance, and love. I could not have done this with out you.

NOMENCLATURE

$5\text{-}HT_3$	5-Hydroxytriptamine Receptors
[A]	Concentration of Substrate / Ligand that Binds Receptor Active Site
A	Substrate / Ligand that Binds Receptor Active Site
BsPFK	Phosphofructokinase from Bacillus stearothermophilus
BsATC	Crystal Structure of the Activated Ternary Complex of BsPFK Bound to F6P, MgADP (Catalytic Site), and MgADP (Allosteric Site).
BsPG	Crystal Structure of BsPFK Bound to PEP
BZ	Benzodiazepine Binding Site
CaSR	Calcium Sensing Receptor
$\Delta\Delta G_{ax}$	Change in Coupling Free Energy Between Substrate and Allosteric Activator
$\Delta\Delta G_{ay}$	Change in Coupling Free Energy Between Substrate and Allosteric Inhibitor
ΔG_{ax}	Coupling Free Energy Between Substrate and Allosteric Activator
ΔG_{ay}	Coupling Free Energy Between Substrate and Allosteric Inhibitor
ΔH_{ax}	Coupling Enthalpy Between Substrate and Allosteric Activator
ΔH_{ay}	Coupling Enthalpy Between Substrate and Allosteric Inhibitor
ΔS_{ax}	Coupling Entropy Between Substrate and Allosteric Activator
ΔS_{ay}	Coupling Entropy Between Substrate and Allosteric Inhibitor
CEPA	2-Carboxyethylphosphonic Acid
CML	Chronic Myeloid Leukemia
E	Enzyme
EA	Binary Complex of Enzyme and Substrate
EcApo	Crystal Structure of apo EcPFK
EcATC	Crystal Structure of the Activated Ternary Complex of EcPFK Bound to FBP, MgADP (Catalytic Site), and MgADP (Allosteric Site).
ECD	Extracellular Domain
ECL	Extracellular Loop

EcPFK	Phosphofructokinase from Escherichia coli
EcPEP	Crystal Structure of EcPFK Bound to PEP
EDTA	Ethylenediamine Tetraacetic Acid
EPPS	N- [2-Hydroxyethyl] Piperazine--3-Propanesulfonic Acid
F6P	Fructose-6-Phosphate
FBP	Fructose-1,6-Bisphosphate
GABAA	γ-Amino Butyric acid A Receptor
GABAB	γ-Amino Butyric acid B Receptor
GPCR	G Protein-Coupled Receptor
GDP	Guanosine 5'-Diphosphate
GlyR	Glycine Receptors
GTP	Guanosine 5'-Triphosphate
ICD	Intracellular Domain
ICL	Intracellular Loop
K_a	Apparent Dissociation Constant of A
K_d	Dissociation Constant
$K_{ia}°$	Dissociation Constant of A in the Absence of Allosteric Ligand
K_{ia}^{∞}	Dissociation Constant of A in the Saturating Presence of Allosteric Ligand
$K_{ix}°$	Dissociation Constant of Allosteric Activator in the Absence A
K_{ix}^{∞}	Dissociation Constant of Allosteric Activator in the Saturating Presence of A
$K_{iy}°$	Dissociation Constant of Allosteric Inhibitor in the Absence of A
K_{iy}^{∞}	Dissociation Constant of Allosteric Inhibitor in the Saturating Presence of A
LGIC	Ligand Gated Ion Channels
MgADP	Magnesium^{2+} Adenosine 5'-Diphosphate
MgATP	Magnesium^{2+} Adenosine 5'-Triphosphate
Mg-dADP	Magnesium^{2+} 2'-Deoxy-Adenosine Diphosphate
MgAMPCP	α-β-Methylene-Adenosine Diphosphate
MgGDP	Magnesium^{2+} Guanosine 5'-Diphosphate
MgIDP	Magnesium^{2+} Inosine 5'-Diphosphate

MgUDP	Magnesium^{2+} Uridine 5'-diphosphate
MOPS	3-[N-Morpholino] Propanesulfonic acid
nAChR	Nicotinic Acetylcholine Receptors
NADH	Nicotinamide Adenine Dinucleotide, reduced form
PDB	RCSB Protein Data Bank
PEP	Phosphoenolpyruvate
PFK	Phosphofructokinase
PG	Phosphoglycolate
Pi	Inorganic Phosphate
PMAA	Phosphonomethylacrylic Acid
PPA	Phosphonoacetic Acid
PTH	Parathyroid Hormone
PTK	Protein Tyrosine Kinase
Q_{ax}	The Coupling Quotient between A and X
Q_{ay}	The Coupling Quotient between A and Y
RMSD	Root-Mean-Square Deviation
RTK	Receptor Tyrosine Kinase
T	Temperature
TM	Transmembrane Domain
TMH	Transmembrane Helix
TK	Tyrosine Kinase
Tris	Tris [Hyroxymethyl] Aminomethane
$v_\circ$	Initial velocity
V	Maximal velocity
[X]	Concentration of Allosteric Activator
X	Allosteric Activator
[X']	Concentration of Allosteric Activator Analog
X'	Allosteric Activator Analog
XE	Binary Complex of Enzyme and Allosteric Activator
XEA	Ternary Complex of Enzyme, Allosteric Acitvator, and Substrate

[Y]	Concentration of Allosteric Inhibitor
Y	Allosteric Inhibitor
[Y’]	Concentration of Allosteric Inhibitor Analog
Y’	Allosteric Inhibitor Analog
YE	Binary Complex of Enzyme and Allosteric Inhibitor
YEA	Ternary Complex of Enzyme, Allosteric Acitvator, and Substrate
ZAC	Zinc Activated Channels

TABLE OF CONTENTS

Page

LIST OF FIGURES

Page

LIST OF TABLES

Page

LIST OF EQUATIONS

Page

1. INTRODUCTION

Each year an estimated $67 billion dollars is spent on research and development for new drugs (*1*), and an estimated cost of $1.3 billion is spent for the development of each new drug (*1*). Given the large investments applied towards research and development, the pharmaceutical industry is always on the lookout for better drug design strategies. Drug design based on allosteric phenomena may provide better strategies than more simple alternatives such as substrate competition. For example, if a disease related protein could be inhibited or activated through allosteric control, a strategy taking advantage of this could grant a greater degree of control over a given physiological system. In the scenario where a physiological molecule is used as a substrate by a variety of proteins, the use of allosteric ligands as the model for drug design may provide an opportunity for greater specificity and selectivity in protein targeting. The use of an allosteric ligand also has the advantage of providing control over a protein's maximal velocity and/or substrate affinity, which can limit side effects and overdosing (*2*). Allosteric effector ligands modify the behavior of a given protein instead of attempting to compete with enzymatic substrates, providing the possibility of fine tuning medical conditions using pharmaceutical treatments.

Cell surface receptors have been increasing in popularity as targets for drug design. This complex group of proteins is diverse in physiological function yet maintain many similarities to one another. Cell surface receptors are often split into 3 major classes: G protein-coupled receptors (GPCRs); ligand-gated ion channels (LGICs); and tyrosine kinases

(*3, 4*). A general description of all classes of cell surface receptors is a membrane protein that exhibits a function when triggered by the binding of the appropriate ligand to a binding site termed the orthosteric site. The orthosteric site is somewhat analogous to the catalytic site of an enzyme in that it serves to bind the ligand responsible for protein function. In cell surface receptors the orthosteric site does not catalyze chemical reaction, but instead catalyzes the triggering of the receptor's function. Hereafter, the orthosteric site will be referred to as the receptor's active site. Recent studies on the allosteric properties of these receptors allow researchers to form libraries of allosteric ligands. The data gathered have revealed a greater diversity of allosteric ligands (hereafter referred to as X) than that of the ligands that bind the receptors' active sites (hereafter referred to as A). The knowledge gained about cell surface receptor allostery and its diversity has enabled the design of drugs with greater specificity in drug targeting, even among the isoproteins within the individual super-families (*5*). In an effort to display the necessity of understanding allostery, this chapter will review the major classes of cell surface receptors along with allosteric drugs that have been shown to modulate their function.

Allosteric Study in Receptors

Structurally, cell surface receptors possess three domains; an extracellular domain (ECD) for interaction with ligand A, a transmembrane segment (TM) for signal transmission through the membrane, and an intracellular domain (ICD) for which to propagate a response. Though the four main classes of receptors vary in their overall physiological roles, they all display this basic morphology and therefore utilize very similar functional mechanisms. Since receptors do not catalyze chemical reactions, a simple description of this mechanism is

as follows: A binds to the active site of the receptor commonly located in the ECD or TM; the binding of A triggers a structural change in the receptor; and the structural change allows for either the up or down regulation of receptor function. For example, LGICs allow the passing of a particular ion through a channel in the protein when ligand A is bound. In other words, the binding of ligand A catalyzes the passage of ions through the protein channel of ligand gated ion channel receptors.

The functional mechanism is often explained by the two common enzymatic models, induced fit and conformer stabilization. Induced fit, in this scenario, presumes that the receptor exists in a preferred structural conformation and ligand A, when bound, forces the protein to modify its structure in order to accommodate it (*6*). In turn, the ligand induced change then modifies receptor function. Conformer stabilization, however, says that the receptor is constantly sampling numerous structural conformations at random. In the event of conformer stabilization, a change in receptor function is seen when ligand A preferentially binds to the relevant conformer, thereby selecting it as the primary conformation. In either case, when the binding of A causes a receptor to produce or increase the production of receptor function ligand A is termed an agonist. When a receptor displays a constitutive function that is decreased or stopped, A is termed an inverse agonist. A third scenario exists where A binds but does not cause a change in receptor function. These types of ligands are called neutral agonists and will not be addressed any further.

Much of the research on receptors has focused on the illumination of the functional mechanism for the individual families. As a result, ligand A analogs were the focus of drug design when it came to receptors. During the last decade, however, research has shifted toward the allosteric modulation of the functional mechanism. This phenomenon is

displayed when a ligand binds to a site that is separate and distinct from the active site of a receptor, the allosteric site, and causes a modulation in the ability of A to change the receptor function.

Many receptors have been shown to exhibit allosteric events that modulate receptor function (*2, 5, 7-12*). Allosteric ligands have been shown to affect receptor function triggered by ligand A in both positive and negative manners. When an allosteric ligand, X, increases the efficacy of ligand A it is termed an activator and an allosteric ligand with a negative impact on the efficacy of A is an inhibitor. Referring to the LGIC example given on the previous page, the binding of X modifies the efficacy by which ligand A triggers the passage of ions through the receptor. Efficacy of ligand A is affected by the allosteric ligand modifying ligand A affinity and/or the modification of ligand A regulated receptor function. Such modulations are described more commonly by the Ternary Complex Model (TCM), which was first proposed to be used in the description of receptors by Lefkowitz et al. and explored more thoroughly by Ehlert (*2, 13, 14*).

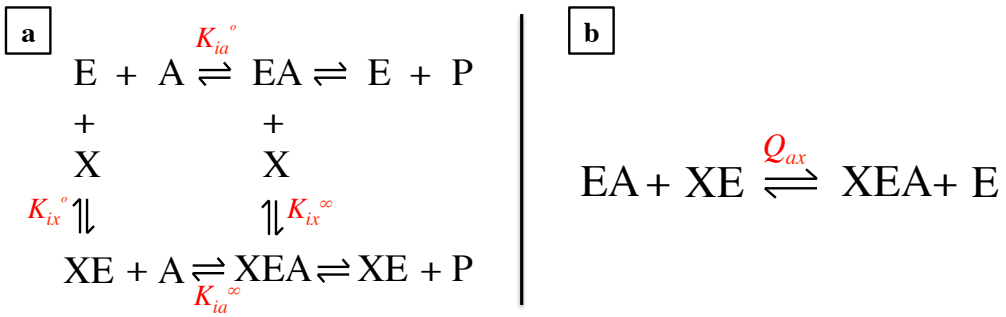

Figure 1-1: a) A diagram for the thermodynamic box representing single substrate, single effector scheme. b) The equilibrium equation for the disproportionation reactions implied by the thermodynamic box in A (*15, 16*).

$$K_{ia}^{o}/K_{ia}^{\infty} = K_{ix}^{o}/K_{ix}^{\infty} = Q_{ax}$$

<u>Equation 1-1:</u> The coupling quotient (Q_{ax} or Q_{ay}) as defined by the apparent dissociation constant of ligand A (in the absence and saturating presence effector X) and the apparent dissociation constant of effector X (in the absence and saturating presence ligand A).

$$\Delta G_{ax} = -RT ln Q_{ax}$$

<u>Equation 1-2:</u> The relationship of the coupling quotient (Q_{ax} or Q_{ay}) to the free energy of coupling (*17*). Note that ΔG_{ax} is a standard state free energy ($\Delta G°$) and that we have deviated from the standard notation.

The nature and magnitude of an allosteric response is better described by thermodynamic linkage analysis (*15, 16*). Here, we will apply this analysis to a single-substrate-single-effector kinetic scheme (Figure 1-1) (*17*). The scheme used assumes that A and X bind at two separate and distinct binding sites on the receptor (E). The scheme provides for two distinct dissociation constants for each ligand, A or X, found in the absence, K_{ia}° and K_{ix}°, and in the saturating presence, K_{ia}^{∞} and K_{ix}^{∞}, of the other, respectively (*15, 16*). The scheme shows the dependence of K_{ia} on [X]. The thermodynamic box implies a reciprocity to the linkage that exists between the substrate and effector ligand. The energy required to reach the ternary complex (XEA) is independent of the path taken, meaning $K_{ia}^{o}K_{ix}^{\infty}=K_{ix}^{o}K_{ia}^{\infty}$. The constants can then be rearranged into $K_{ia}^{o}/K_{ia}^{\infty}=K_{ix}^{o}/K_{ix}^{\infty}$ (Equation 1-1) which we use to define the coupling quotient (Q_{ax}) (*15, 16*). Q_{ax} represents the nature and magnitude of an allosteric phenomenon, enabling a much more complete characterization of a given allosteric interaction. In the case of an activator, Q_{ax} will have a value greater than one, and for an inhibitor its value is less than one (Equation 1-1) (*18*). Q_{ax} also represents the thermodynamic equilibrium of the disproportionation reaction given in Figure 1-1 and described by equation 1-1 (*15-17*). Since Q_{ax} is an equilibrium constant, it can be used to calculate the free energy of coupling between A and X by equation 1-2.

Modified versions of the thermodynamic linkage model are highly utilized in the detection allosteric modulators in drug development. Due to the simplicity of the model, it can easily be incorporated into common drug research assays, such as radiolabeled probe assays, which are already prominent in the field of receptor studies (*2*). There are two aspects of thermodynamic linkage analysis that allow for its ease of application. The first aspect is the existence of reciprocity between A and X. Although X is perceived to be

allosterically modulating A, thermodynamic linkage analysis states that A is equally modulating X. In this scenario reciprocity allows a certain degree in freedom in experimental design but more importantly allows the second assumption. The second important aspect is that the effect of allostery on binding affinity is shown to be separate from the allosteric effect on efficacy of the functional mechanism.

G Protein-Coupled Receptors

The largest class of cell surface receptors is the G protein-coupled receptor (GPCR) superfamily with well over 1000 members (*19*). G proteins are heterotrimeric guanine nucleotide binding proteins that interact with and regulate intracellular targets in response to extracellular signals. GPCRs are known to be involved in the physiological functions of taste, smell, and sight via their recruitment and regulation of G proteins (*3*). G proteins have 3 subunits that are denoted as α, β, and γ. When the α subunit is bound to guanosine diphosphate (GDP) it binds to the intracellular carboxy-terminus of a GPCR. The general functional mechanism of a GPCR begins with the binding of ligand A, a neuropeptide or peptide hormone, to the active site. Once bound the GPCR changes conformation, which is then propagated through the plasma membrane and to the G protein α subunit. The conformational shift of the G protein now allows for the dissociation of GDP followed the binding of GTP. Once GTP is bound the α subunit dissociates from the GPCR and the other G protein subunits. The left over subunits now

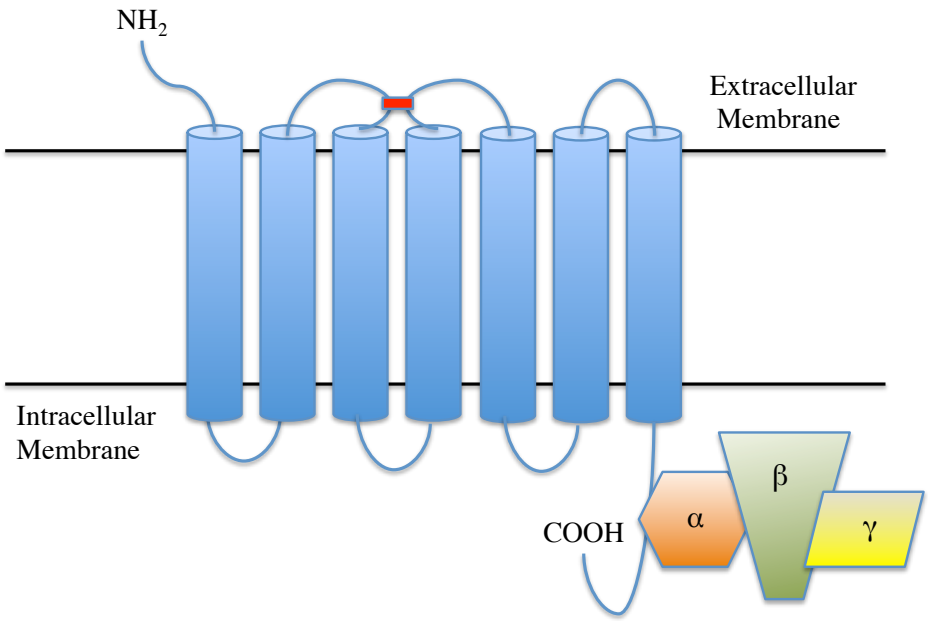

<u>Figure 1-2:</u> Representation of a GPCR showing seven transmembrane helices (TMH), three extracellular loops, three intracellular loops, the α G-protein bound to the C-terminus region in orange, the β G-protein in green, and the γ G-protein in yellow. The disulfide link between ECL1 and ECL2 is represented in red.

form the βγ G protein and go on to interact with intracellular targets along with the GTP bound α G protein. Once the α subunit associates with various targets that can hydrolyze the GTP to GDP, the α reassociates with βγ and the GPCR carboxy-terminal (*3*).

GPCRs exist as homo and hetero pentamers. The major structural characteristic of GPCRs is the possession of 7 transmembrane helices (TMH). The monomeric proteins are oriented so that the amino-terminals are extracellular and the carboxy-terminals are intracellular. GPCRs also possess 3 extracellular and 3 intracellular loops (ECL and ICL, respectively). Another overall GPCR characteristic is a conserved disulfide link between ECL1 and ECL2 (Figure 1-2) (*19*). As a whole the GPCR superfamily shares little sequence homology, except when it is sub-divided into families (*19*). Most commonly, GPCRs are divided into 3 families using phylogenetics and sequence homology (*20*).

Class A, Rhodopsin-Like Receptors, is the largest GPCR family with over 800 members (*20, 21*). Overall sequence homology among class A GPCRs is still low with the exception of an Aspartate-Arginine-Tyrosine (DRY) motif that appears in ICL2 (*20*). Class B, Secretin-Like Receptors, is considerably smaller with around 40 receptors. This family is characterized by a larger amino terminus containing several, highly conserved, cysteine residues (*20, 21*). Last is Class C, Metabotropic and γ-Amino Butyric Acid Receptors. This group consists of around 200 members and is characterized by a 500-600 residue amino-terminus, the largest of the GPCRs. The ECD of class C GPCRs is predominantly comprised of the amino-terminus. This large ECD is often described as a venus fly trap of which the ligand A binding site lies in the middle (*12, 20*).

Cell Surface receptors are thought to be the target for more than 40% of the nearly 1400 unique drugs that have been approved by the FDA (*22*). Of that 40%, GPCRs account

for 67% of the targets. In fact, the last 25 years of research have shown drugs like aspirin, heparin, and zinc to be allosteric modulators of GPCRs and they have been in use for decades (*12*). However, as stated previously, there are many new allosteric drugs in development that are targeted towards cell surface receptors. One example of the relatively new drugs is maraviroc.

Maraviroc is an allosteric inhibitor of the chemokine receptor CCR5 (*23*). CCR5 is a Class A GPCR that is expressed in T-cells and other leukocytes, and is involved in the chemotaxis of these cells. CCR5 ligands are the chemokines RANTES, MIP-1β, MIP-1, and MIP-2 (*24*). This particular chemokine receptor, along with CXCR4, has garnered a great deal of attention in recent years due to their participation in the HIV-1 infection process. This attention has also been driven by the discovery of the non-life threatening variant CCR5Δ32. Many of the common HIV-1 strains utilize CCR5 and/or CXCR4 as co-receptors to gain cell entry. The CCR5Δ32 variant is a 32 base pair deletion in the gene of CCR5 that results in the premature termination of CCR5 production. CCR5Δ32 results in receptor proteins terminated between TMH4 and TMH5. The end result of this deletion is an absence of CCR5 expression and a highly HIV-1 resistant homozygous population (*23, 25*). Traditional drugs, such as competitive inhibitors, that have been investigated for CCR5 inhibition have been discouraging due to a lack of finite specificity. CCR5 belongs to sub-family of 19 total receptors that bind to chemokines, resulting in a high degree of sequence homology in the extracellular orthosteric ligand binding site (*21*). In this case a drug that does not have a high specificity for just CCR5 can cause severe immune depression by inhibiting other critical receptors such as CCR2 and CXCR4 (*23*). Maraviroc has displayed the characteristics of a typical allosteric inhibitor for GPCRs and has shown the ability to

selectively inhibit only CCR5 (*23*). This type of allosteric regulation allows patients to effectively display the Δ32 phenotype while allowing normal immune function to continue (*23*). Maraviroc displays a potential strength for all allosteric drugs in the ability to regulate a specific protein without affecting its homologous family members.

Cinacalcet is another example of allosteric strengths utilized in GPCR drug function. Cinacalcet is a known allosteric activator of Calcium Sensing Receptor (CaSR) (*26*). CaSR is member of Class C GPCRs and is responsible for the monitoring and regulation of calcium in the body. CaSR are located on the surface of parathyroid chief cells and are bound to Ca^{2+} when they are non-functional. When serum Ca^{2+} levels become too low Ca^{2+} dissociates, triggering CaSR to release parathyroid hormone (PTH) (*26*). PTH acts to increase Ca^{2+} levels by stimulating the reabsorption of calcium from bone and kidney filtrate. High serum Ca^{2+} levels are commonly caused by secondary hyperthyroidism, and often seen in patients with reduced kidney function (*26*). Since Cinacalcet is an allosteric activator of CaSR it is often used to treat such patients in order to increase sensitivity of CaSRs calcium detection. In other words, cinacalcet better enables CaSR to do its job. Drugs like cinacalcet attempt to allow the body's natural regulation to control Ca^{2+} instead attempting to take over Ca^{2+} homeostasis via multiple drugs or treatments (*27*).

Ligand Gated Ion Channels

Ligand gated ion channels (LGIC) were first isolated from the electric organ of *Electrophorus electricus* in 1970 (*28*). Since their discovery, LGIC receptors have been shown to express in every animal cell and proven to be a necessity in brain function due to their regulation of ion passage through membranes. Although the majority of cells express

LGICs in small numbers, they can cover nearly 50% of nerve cell membranes (*29*). Given their function and population density on nerve cells it comes as no surprise that LGICs are critical in fast synaptic transmission. The basic mechanism of LGIC receptor function is the binding of a neurotransmitter to the active site in the ECD, triggering a conformational shift that opens the receptor pore allowing ions to pass (*30*).

LGICs can be structurally quite different and are sub-divided based on these structural differences alone. Commonly, there are 3 super-families; the cys-loop superfamily, the ATP gated channel superfamily, and the glutamate activated cationic susperfamily (*31*). Given that LGICs traffic ions they are all also recognized as being either excitatory-cation selective, or inhibitory-anion selective (*10*).

Cys-loop receptor superfamily is the largest of the three LGIC superfamilies and will be the only superfamily discussed further. All the LGICs are homo and/or hetero oligomeric channels, with the families often discussed in terms of their monomeric proteins that form the channels (*10, 32*). The cys-loop superfamily contains 47 identified monomeric proteins that form 5 types of homo/hetero pentameric channel receptors. Each type of receptor utilizes a specific number and set of monomeric proteins as subunits. Nicotinic acetylcholine receptors (nAChR) use 17 monomers while 5-hydroxytriptamine receptors (5-HT_3), zinc activated channels (ZAC), γ-amino butyric acid A and B receptors ($GABA_A$ and $GABA_B$), and glycine receptors (GlyR) use 5, 1, 19, and 15 subunits, respectively (*31, 32*). Of this superfamily only the GABA receptors and GlyR are anion selective, while the remainder of superfamily is cation selective. All cys-loop receptors retain a characteristic loop in the ECD, composed of the amino-terminus. This "Cys-Loop" is a 13 residue segment flanked by 2 cysteine residues that form a disulfide bond with one another. The rest of the ECD, which contains

the active sites, is primarily composed of β-sheets. The 3 LGIC superfamilies all have a different number of transmembrane segments and the cys-loop superfamily has 4 transmembrane helices that help form the ion channel (*30*). The carboxy-terminus structure composing the ICD is largely unknown except for the existence of an α-helix that resides at the opening of the channel pore (Figure 1-3).

With GPCRs supplying the targets for 67% of the 40% cell surface receptor drugs, the vast majority of the remaining 33% are targeted towards ligand LGICs (*22*). Drugs targeted towards LGICs are known to treat disorders and diseases such as epilepsy, insomnia, nicotine addiction, ADHD, depression, and Crohn's disease (*33*). The disorders and diseases listed are thought to be caused by genotypes that cause channels to open too slowly, close to slowly or close to quickly (*33*). Since the purpose of allostery is to regulate proteins, allosteric drugs are the logical choice for treatment of LGIC disorders.

With a large number of subunits belonging to each LGIC superfamily, the formation of heteromeric channels is common. LGICs are able to somewhat differentiate themselves physiologically from one another due to their active sites being located at the subunit interfaces making multiple configurations possible. With the variety of possible configurations it is not uncommon to see some active sites serving as allosteric sites and lose the ability to directly trigger channel gating (*11*). The subunit that contributes the majority of the ligand binding site is called the principal subunit. The subunit that contributes the remaining portion of the binding site is termed the complementary subunit (*30*).

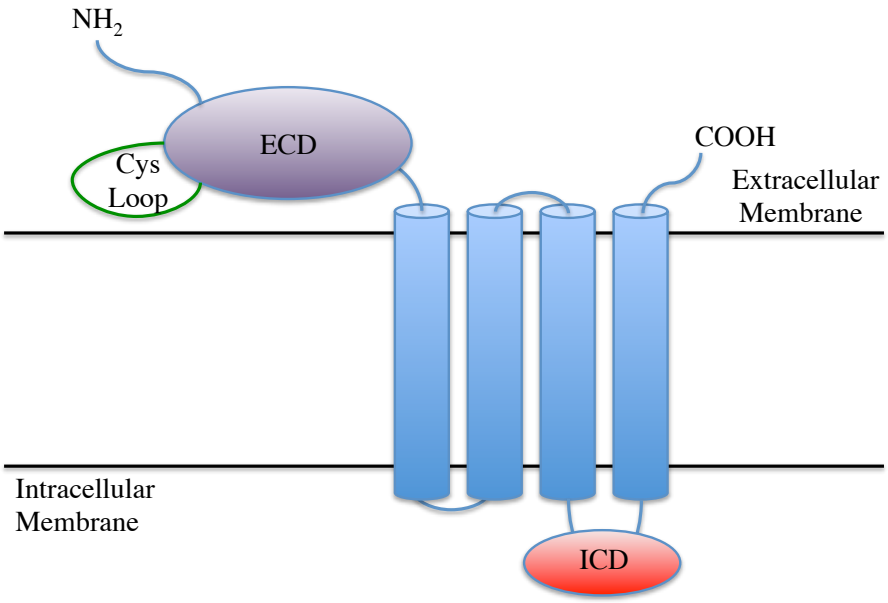

<u>Figure 1-3:</u> Representation of the Cys-Loop superfamily of ligand gated ion channel showing the Cys-loop in green, four transmembrane helices (TMH) in blue, an extracellular domain (ECD) in purple, and an intracellular domain (ICD) in red.

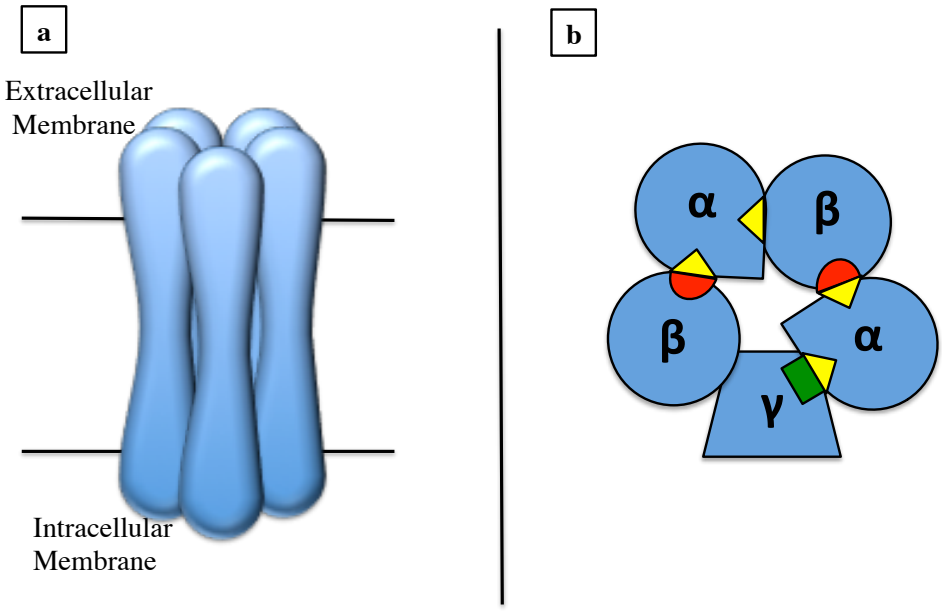

Figure 1-4: a) Idealized representation of receptor monomer grouping, b) Top down view of receptor monomers α, β, and γ. The αβ ligand A binding sites are comprised of a yellow α portion and a red β portion. The αγ allosteric site is comprised of a yellow α portion and a green γ portion.

The interaction of benzodiazepines with the αβγ$GABA_A$ receptor, member of the cys-loop superfamily, is considered a classic example of allosteric sites derived from former active sites (*12, 32*). αβγ$GABA_A$ receptors are inhibitory anion selective receptors and are most common $GABA_A$ subtype found in the brain (*34*). Benzodiazepines have been approved drugs and on the market for over 50 years. Just a few examples are alprazolam (Xanax), clonazepam (Klonopin), and diazepam (Valium). Benzodiazepines are used to treat a very long list of afflictions that includes epilepsy, anxiety disorders, sleep disorders, and skeletal muscle pain/spasms (*34-36*).

The αβγ$GABA_A$ receptor is composed of two α, two β, and one γ $GABA_A$ subunits and ordered as shown in figure 1-4. The active site is formed at the βα interface, that is where β is the principal and α is the complementary subunit. The allosteric site, or benzodiazepine binding site (BZ) in this scenario, is located at the αγ interface, where α now serves as the principal subunit. The γ subunit, unlike the β subunit, prevents the ligand binding site formed with the α subunit from directly triggering receptor function, but allows it to function as an allosteric site. This composition and arrangement of subunits yields 2 active sites and one allosteric site (*11*). When benzodiazepines are bound to the αγ ligand binding site they have been shown to modulate both active site affinity for ligand A and the ability of ligand A to trigger receptor function (*2, 34, 37*). More recently studies have been attempting to parse out the residues involved in binding specificity and allosteric modulation in order to design better and more specific benzodiazepines (*34*).

Tyrosine Kinases

The third and last major group of cell surface receptors is the tyrosine kinase (TK) superfamily. This superfamily has gained a substantial amount of attention since their discovery in 1980 (*38*). TKs are subdivided into two superfamilies; receptor tyrosine kinases (RTK) and protein tyrosine kinases (PTK). TKs possess a large amino-terminus that composes the ECD along with the active site. Displaying the least number of transmembrane segments out of all receptors discussed, RTKs only possess one. The carboxyl-terminus is intracellular and contains a catalytic site which displays tyrosine phosphorylating activity (Figure 1-5a) (*3*). Although the description just given is true for TKs, stipulations must be made for PTKs. Unlike RTKs, PTKs rely on their close association with cytokine receptors. PTKs are analogous to the catalytic portion of RTKs, while cytokine receptors are analogous to the transmembrane and receptor portions of RTKs. The physiological mechanism of the heteromeric receptor is also analogous to RTK (*3*). For the purposes of this discussion, an RTK monomer is comprised of a single protein and a PTK monomer is comprised of two proteins, a membrane/transmembrane subunit and a catalytic subunit.

Despite the slight difference in structural composition, these two families function with extremely similar mechanisms and will be assumed identical for the following discussion. TKs utilize multiple controls in order to assure control over their cellular functions. The first of these controls is that TKs exist in the membrane as monomers when unbound by active site ligand. When the appropriate cell signal molecule binds the receptors, it induces dimerization. The active site signaling ligand acts as a cross-linker as well as an

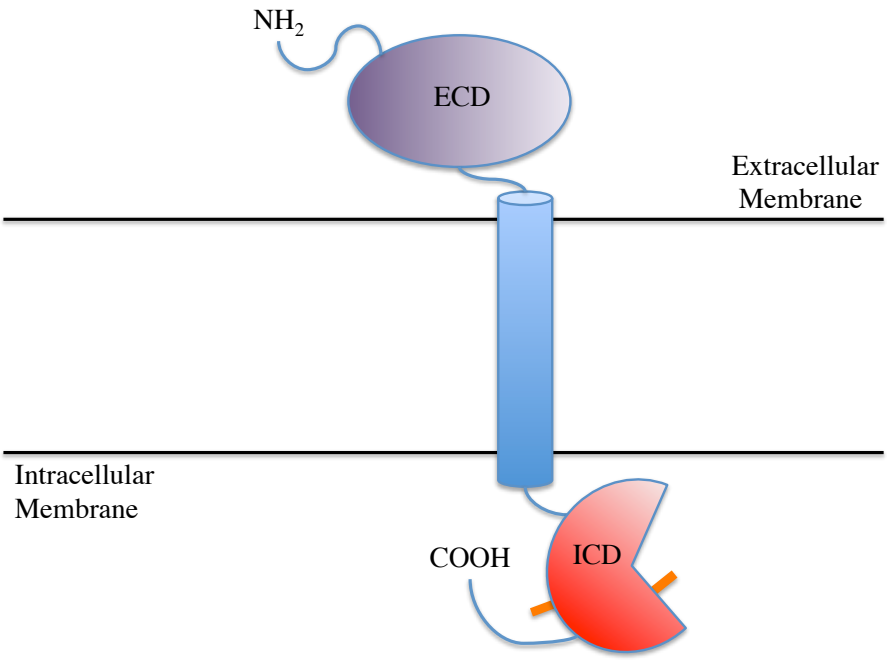

<u>Figure 1-5a:</u> Representation of the Tyrosine Kinase superfamily of ligand gated ion channel showing one transmembrane helix in blue, the extracellular domain in purple, and the intracellular domain in red. Orange rectangle represent potential phosphorylation sites.

allosteric ligand to promote dimerization and therefore induce activation (*3, 39*). Once activated TKs autophosphorylate one another twice within their ICDs (Figure 1-5b). Once on a loop in the catalytic domain called the activation loop, to increase kinase activity, and again outside the catalytic domain to create a binding site for intracellular signaling proteins (*3*). Autophosphorylation for increased catalytic activity is a result from a ligand activated receptor dimer and is thought to help auto-inhibit in the event of a random dimerization (*39*).

TKs have been shown to play crucial roles in cell growth, proliferation, differentiation, and immune response. The development of cancer has been described as an imbalance between cell cycle progression, mass, and apoptosis (*40*). Given the two previous statements it is no wonder that mutations in TK genes make up a large group of oncogenes (*41*). Even the discovery of TKs is because of research to identify oncoproteins (*38*). Imatinib (Gleevec), and many of its derivatives, is an FDA approved drug that specifically targets certain TKs (*42-44*). Imatinib has been shown to only affect the tyrosine kinases designated as Abl, Kit, and PDGFR (*45, 46*). Imatinib targets the catalytic component of TKs and is considered a selective ATP competitive inhibitor. Imatininb is considered to be selective due to its high affinity and interaction with a hydrophobic pocket adjacent to the catalytic site. Imatininb has also been deemed an ATP competitive inhibitor since the hydrophobic pocket is so close to the ATP binding site that it can utilize the nucleotide binding portion for its own association (*45, 46*). Once bound, the drug "locks" the kinase in an unactivated conformation. This conformation causes the previously mentioned activation loop, which is known to be somewhat free moving, to pull into the catalytic site and interact with the residues that are key in ATP phosphate binding.

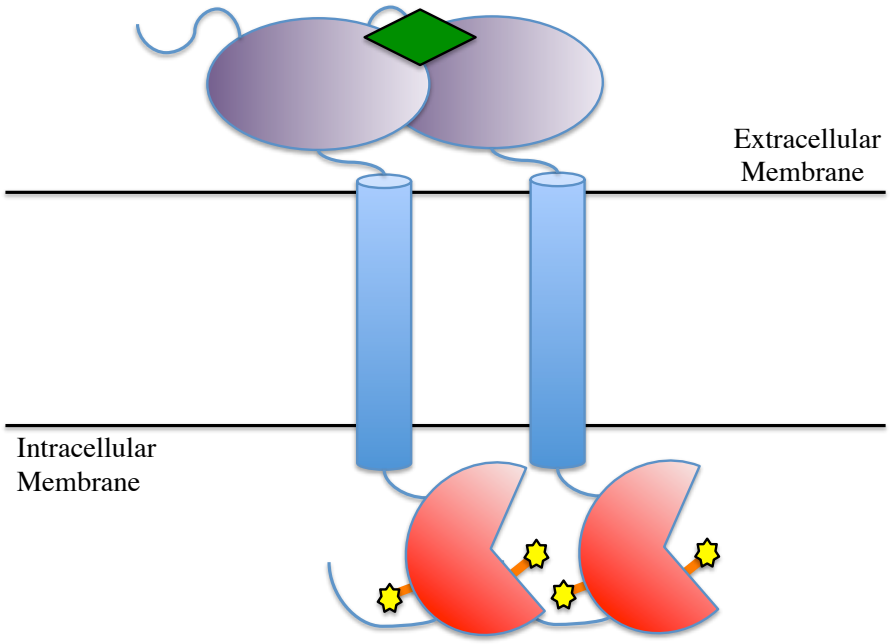

<u>Figure 1-5b:</u> Representation of an activated Tyrosine Kinase superfamily of ligand gated ion channel. The green diamond represents ligand A binding to a dimer of the receptor proteins. Yellow stars represents the phosphorylation of the intracellular domain.

The presence of imatinib and the conformational shift it causes effectively closes the active site preventing the binding of ATP and therefore unregulated kinase activity (*44, 45*).

Chronic Myeloid Leukemia (CML) is a cancer associated frequently with a translocation event that creates the "Philadelphia Chromosome" (Ph). This chromosome contains the breakpoint cluster region Ableson oncogene (BCR-ABL). This gene yields the fusion protein Bcr-Abl. Bcr-Abl is a deregulated PTK with constitutive kinase activity belonging to a normal Abl PTK (*44, 47*). Given that a portion of the fusion protein is Abl made imatinib the logical drug choice. However, nearly all CML patients who were Ph+ developed imatinib resistance, via point mutations in the Bcr-Abl protein, allowing the cancer to rebound (*43, 44, 48*). The point mutations that occurred were all within the hydrophobic binding pocket utilized in imatinib binding. The appearance of the Bcr-Abl point mutations stimulated a search for redesigned imatinib and possibly a drug with an alternative inhibitory action. In recent publications two drugs, GNF-2 and GNF-5, were shown to use the native Bcr-Abl binding sites for myristate as an allosteric site (*43*). This research showed that GNF-2/5 could strongly activate the binding of imatinib to a hydrophobic pocket next to the Bcr-Abl catalytic site in all but one of its known hydrophobic mutations. GNF-2/5 could diminish mutant Bcr-Abl activities equal to that of imatinib with the native Bcr-Abl. The T315I mutation, dubbed the "gatekeeper" mutation, is located within the ATP binding site of Bcr-Abl. T315I disrupts a hydrogen bond that is extremely important to imatinib binding. The gatekeeper mutation decreases GNF-2/5 affinity by half, relative to wild type, and a maximum 20% inhibition relative to the other Bcr-Abl mutations studied (*43*).

The Current Study

In the previous discussion there have been examples of allosteric drugs that display great advantages over typical competitive analogs. Cinacalcet and maraviroc both impact efficacy by increasing and decreasing it, respectively. In particularly, maraviroc shows high selectivity among its most homologous family members. The benzodiazepines which show specificity of target and highlight the fact that allosteric drugs have been in use for decades. Lastly, is the ability of GNF-2/5 to allosterically regulate the binding of imantinab. With the majority of these drugs being discovered in the last 2 decades, the drug development industry appears to be trending towards the development of allosteric drugs (*11, 27, 42, 49, 50*).

Important steps in drug design for cell surface receptors came due to advances in fundamental research. As displayed by the imatinib and GNF2/5 research, understanding the underlying biochemical and biophysical mechanisms of a target cannot and should not be avoided. Even though GNF-2/5 was presented as a solution, the Zhang et al. expressed confusion and intrigue as to why the gatekeeper mutation has a low maximal effect (*43*). Further, Zhang et al. hypothesized that the gatekeeper residue could be somehow coupled to GNF-2/5 binding but also concluded that the gatekeeper residue simply does not favor the inactivate conformation (*43*). The utilization of fundamental research in drug design can release investigators from oversimplifications and preconceived models that are the basis of modern high throughput screening drug design. The current high throughput approach to development still takes between 10 to 15 years for a drug to go from screening to FDA approval (*51*). Given the amount of time spent in development it may come as no surprise that the average cost of drug development is steadily increasing. The cost to develop increased over 2-fold from the years 1987-2001 but nearly achieved the same increase from

2001-2005 (*1*). While there is no doubt that, in a fast paced industry, high throughput design has great merit, there has never been a more obvious need for a thorough understanding of allostery. More specifically, there is a need to better understand the effect of allosteric ligand structure on the characteristics of the resulting allosteric behavior. The relationship between ligand structure and allosteric function is key to the advancement of allosteric based pharmaceutics.

Here I attempt to better understand the relationship between allosteric ligand structure and the resulting allosteric behavior by investigating the roles that functional groups and structure play in the binding affinity and allosteric potency of ligands at the allosteric site of phosphofructokinase from E. coli (EcPFK). EcPFK catalyzes the conversion of fructose-6-phosphate (F6P) into fructose-1,6-bisphosphate (FBP) via phosphoryl transfer from MgATP. EcPFK is allosterically inhibited and activated in the presence of phospho-enol-pyruvate (PEP) and MgADP, respectively. EcPFK also displays very strong homotropic coopertivity towards F6P when MgATP is bound. Both activator and inhibitor have been shown to bind to the same effector site and result in only K-type effects. The fact that both MgADP and PEP bind to the same binding site using a majority of the same residues, makes EcPFK an ideal system for this type of allosteric characterization.

In chapter II, I describe a study of the crystal structure of EcPFK that has been solved with PEP bound to the allosteric binding sites (EcPEP). Over the years, the two state model has been relied upon to explain allosteric behavior of EcPFK. The use of the two state model has seemingly been justified due to the two published crystal structures of EcPFK and the earlier crystal structures of its homolog, *B. stearothermophilus* PFK (BsPFK) (*52-54*). The known EcPFK publications represent the enzyme in the apo form (EcApo) and the activated

ternary complex form (EcATC). The EcATC is bound to FBP and MgADP in the active site, as well as MgADP in the effector site (*55, 56*). Thermodynamic linkage analysis allows the consideration of the enzymatic forms set forth by the disproportionation equilibrium in figure 1-1b. In the scheme presented in figure 1-1b, E represents the apo form of an enzyme; XEA (or YEA if an inhibitor) represents the ternary complex between allosteric ligand (X or Y), enzyme (E), and substrate (A); EA represents the binary complex between enzyme and substrate; and XE represents the binary complex between allosteric ligand and enzyme. For EcPFK, only two of these enzymatic complexes have had their crystal structures solved and reported. EcApo represents E in the disproportionation equation and EcATC represents the only ternary complex, XEA, reported for EcPFK. Chapter II presents the first study of the YE complex of EcPEP and the first reported crystal structure of any EcPFK and allosteric ligand binary complex.

Chapter III is a thorough kinetic characterization of the coupling between fructose-6-phosphate (F6P) and allosteric effector analogs. The resulting study suggests the role of functional groups belonging to allosteric ligands. Different effector analogs that vary only slightly from the natural allosteric effectors of EcPFK were utilized. The minor modifications of effector analog relative to effector, allow for meaningful comparisons of the parameters obtained via thermodynamic linkage analysis with F6P and allosteric ligand. Comparison of dissociation constants (K_d) between the effectors and effector analogs allows for a direct analysis of the affects on binding affinity by the variation present, whereas the comparison of the coupling quotient (Q_{ax}) yields the impact on allosteric response. Chapter III further interrogates the interactions between ligand and protein via modification of effector site residues. In effect, one could reason that the ligand analog study mentioned in

the previous paragraph entailed the “mutation” of effector ligands in order to differentiate the functional constituents from their molecular structure. Using the information obtained from the ligand analog study along with what is known about the effector binding site, more conclusions were made about ligand-residue interactions in the effector site. Modification of ligand interacting residues results in altered allosteric response in a manner comparable to those seen with the modified effectors and wild type enzyme.

2. CRYSTAL STRUCTURE

Introduction

Glycolysis is a very important metabolic pathway that is responsible for converting glucose to pyruvate. This conversion creates ATP and NADH which is needed for cellular function. The first committed step of glycolysis is catalyzed by the allosteric enzyme, phosphofructokinase (PFK). PFK from *Escherichia coli* (EcPFK) is a long standing and well established model for the study of allosteric phenomena. EcPFK is catalytically active as a homotetramer with each monomer comprised of 320 amino acids. The tetramer is approximately 140kDa in size and has four identical catalytic sites and four identical allosteric sites that all lie on the interfaces between monomers (*57*). EcPFK is inhibited by the glycolytic product phospho-enol-pyruvate (PEP) and activated by its product MgADP. Both PEP and MgADP produce K-type effects only. EcPFK catalyzes a phosphoryl transfer from ATP to convert fructose-6-phosphate (F6P) into fructose-1,6-bisphosphate (FBP). The symmetry and relative simplicity of EcPFK combined with thermodynamic linkage analysis allows the use of a single substrate, single modifier scheme for characterization (*15, 16, 58*). EcPFK analysis in this manner allows for the assignment of meaningful allosteric parameters. For example, the coupling quotient (Q) depicts the nature and the magnitude of a particular allosteric interaction (*15, 16*). This same symmetry, however, also lends itself to preconceived assumptions and models as concluded in the original EcPFK characterization in 1968 (*57*). The conclusion of Blangy *et al.* used the simplicity of a one substrate, one

modifier model to suggest that the allostric properties of EcPFK can be qualitatively and quantitatively accounted for by the 2-state Monod, Wyman, and Changeux model (*59*).

There are two X-ray crystal structures of EcPFK that have been published. The first EcPFK structure reported was of the activator bound ternary complex (EcATC) which has fructose 1,6-bisphosphate (FBP) bound to the catalytic site, MgADP bound to the catalytic site, and MgADP bound to the allosteric site (PDB entry 1PFK) (*55*). This EcATC structure was concluded to represent the "R-state conformer", consistent with the hypothesis that EcPFK can be described by a 2-state model (*55*). The second structure reported was the apo structure (EcApo) of the enzyme (PDB entry 2PFK) (*56*). Contrary to the prediction of Blangy *et al.* (*57*), Evans *et al.* concluded that the EcApo structure, represents the "R-state conformer" of EcPFK. Evans also noted that EcApo did not display the expected quaternary structure shift first identified by their group in 1986 (*60*). The 1986 publication reported *Bacillus stearothermophilus* phosphofructokinase (BsPFK) with the analog inhibitor 2-phosphoglycolate bound at the allosteric sites but unfortunately had a low 7Å resolution (PDB entry 5PFK) (*60*). BsPFK, like EcPFK, is a homotetramer with four identical catalytic sites, four identical allosteric sites (*52, 61, 62*). The monomers of BsPFK consist of 319 residues and share a 55% amino acid sequence identity with the 320 residues of EcPFK (*62*). This isoenzyme is activated and inhibited by MgADP and PEP, respectively (*52*) as well.

In 1990 Evans *et al.* published yet another BsPFK crystal structure. The structure published was a 2.5Å resolution BsPFK structure bound to 2-phosphoglycolate (BsPG) depicting a high resolution "T-state conformer" (PDB entry 6PFK) (*53*). Evans also published BsPFK with F6P and MgADP bound to the catalytic site as well as MgADP to the allosteric site (PDB entry 4PFK), yielding the structure of the activator bound ternary

complex (BsATC) (*52*). The series of EcPFK and BsPFK crystal structure publications by Evans *et al.,* combined with the high structural similarity between the two isoenzymes, has lead some groups to use BsPG as a guide for EcPFK research (*63-68*).

BsPFK is a completely different enzyme with a completely different set of allosteric and kinetic parameters. The F6P affinity reported for BsPFK is 10 times higher than that of EcPFK. Also, when considering F6P binding, EcPFK displays very strong F6P homotropic cooperativity while BsPFK shows very little in the presence of MgATP. Allosteric coupling between F6P and PEP for BsPFK is more than 10-fold greater than EcPFK. The van't Hoff analysis of each enzyme shows that the free energy of allosteric coupling (ΔG_{ax}) for BsPFK is driven by the entropic ($T\Delta S_{ax}$) component while EcPFK is dominated by the enthalpic (ΔH_{ax}) contribution (*17, 18, 69, 70*). Using the allosteric behavior displayed by BsPFK as an explanation of the allosteric inhibition displayed by EcPFK, is a rough approximation at best. The BsPG structure not only features an enzyme that is not EcPFK, but also an analog of the native allosteric inhibitor. Though no kinetic data were published, 2-phosphoglycolate (PG) was reported to have a weak affinity for BsPFK but to yield the comparable kinetic effects to that of PEP (*53*). Later studies showed that BsPFK affinity for PEP is 10 times stronger than PG and the allosteric coupling between F6P and PG is 10-fold greater (*71*). In this report we present the crystal structure of EcPFK with PEP bound to the allosteric sites at a 2.8Å resolution (EcPEP). EcPEP is the first reported EcPFK structure with any inhibitor bound. EcPEP is also the first known crystal structure of any wild type bacterial PFK bound to its physiological allosteric inhibitor (Figure 2-1).

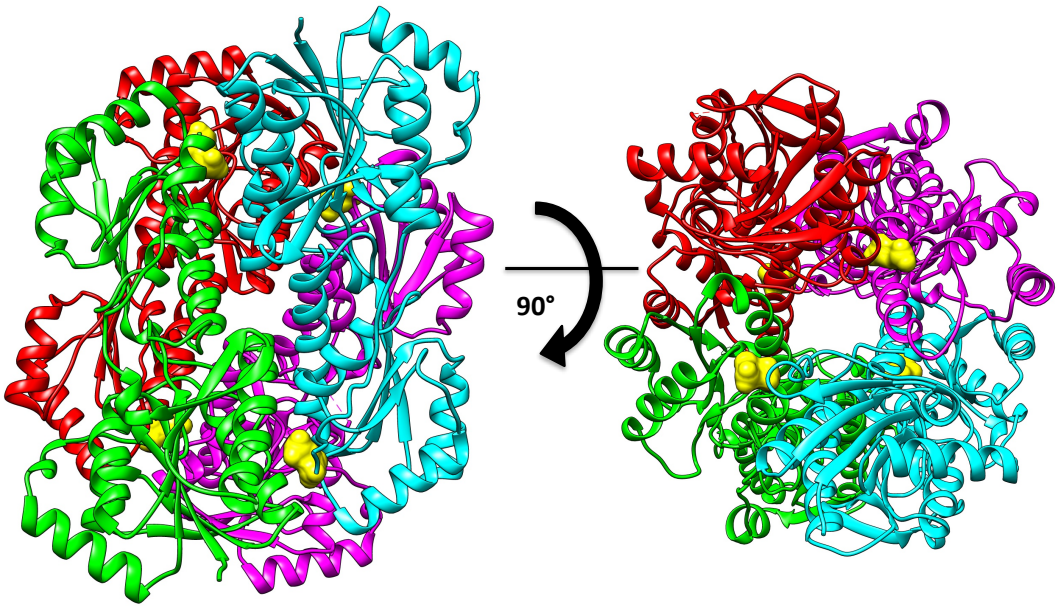

Figure 2-1: Two views of the crystal structure for EcPFK with PEP bound to the effector site. Peptide chains are represented as ribbon structures and PEP is represented as yellow surface fill structures. Left is a side view if the structure, and right is a top down view.

Materials and Methods

Enzyme Source and Purification

Wild type E. coli PFK-1 gene, as described previously (*72*), was expressed from the pGDR148 plasmid which was transformed into competent RL257 cells (MQ ΔpfkB :: FRT ΔpfkB:: ΔpfkA, MQ is a lac+ laqiq derivation of MC4100), a PFK-1 and PFK-2 deficient strain (*73*). Once transformed into RL257, the EcPFK producing cells were stored at -80 ºC in a glycerol solution consisting of 50% glycerol, 50 mM TRIS HCl pH 7.5, 5 mM $MgCl_2$, and 0.1 mM EDTA. The purification of EcPFK was purified according to the methods of Johnson et al. with modifications (*74*). The frozen cells were resuspended in 50 mL of TRIS Purification Buffer (50 mM Tris-HCl pH 7.5, 5 mM $MgCl_2$ and 0.1 mM EDTA). Cells were lysed by sonication using a Sonic Dismembrator Model 550 (Fisher Scientific). The sonication protocol consisted of fifteen-second pulses followed by a one-minute rest period to allow the cells to cool. A total sonication time of 8 minutes was used. The crude lysate was clarified by centrifugation at 12,000 RPM for 60 minutes in a Beckman J2-21 centrifuge. The pellet was discarded.The supernatant was incubated in the presence of deoxyribonuclease I at 37 °C for 15 minutes and then centrifuged for 60 minutes. The supernatant containing EcPFK was then diluted to 120 ml using Buffer A (50 mM Tris-HCl pH 7.5, 5 mM $MgCl_2$, 0.1 mM EDTA, and 100 mM NaCl). The 120 ml supernatant containing EcPFK was then loaded onto a column containing a 40 ml bed volume of Mimetic Blue 1 agarose resin, from Prometic Biosciences (Rockville, MD), equilibrated with Buffer A. The supernatant was loaded onto the column at a rate of 2 ml/min. After the supernatant was loaded any unbound protein and/debris was washed from the column using 800 to 1000 mL of Buffer A, or until the pass through from the column had an absorbance of approximately 0.012 at 280 nm. EcPFK was

then eluted using a gradient of Buffer A and Buffer B (50 mM Tris-HCl pH 7.5, 5 mM $MgCl_2$, 0.1 mM EDTA, and 2.5 M NaCl) over 200 ml. Fractions were collected in 10 ml increments and checked for PFK maximal activity and A280 reading. The fractions having enzymatic activity and low contamination were pooled together as one sample. The pooled sample was then dialyzed against TRIS Purification Buffer and concentrated using Amicon Ultra-15 (100K). The concentrated sample was then dialyzed against EPPS storage buffer (50 mM EPPS pH 8.0, 10 mM NH4Cl, 10 mM $MgCl_2$, and 0.1 mM EDTA). SDS-PAGE was performed and used to check the EcPFK purity. Protein concentrations were determined using the BCA protein assay reagent (*75*). Absorbance readings using $\varepsilon 278 = 0.6\ cm^2mg^{-1}$ (*76*) were taken and they agreed with BCA determined protein concentrations. PEP was then added to the EcPFK in EPPS storage buffer, for a total concentration of 5 mM PEP and a final concentration of 15.7 mg/mL for EcPFK.

Crystallization and Data Collection

EcPFK bound to PEP was crystallized using the hanging drop vapor diffusion method at 16°C (*77*). Crystallization was achieved in a 5 µl drop consisting of 1.5 µl of buffer (0.1 M HEPES pH 7.5, 0.1 M spermidine, 8% v/v propanol, and 18% w/v polyethylene glycol 8,000) and 3 µl of protein (stock concentration of EcPFK was 15.7 mg/mL with 5.1 mM PEP). The resulting EcPFK crystals were soaked in 30% ethylene glycol and then flash-frozen in a liquid N2 stream at 100 K. The diffraction data were then collected on an APS beam line 23-ID (insertion device) using a MAR 300 CCD detector (MarMosaic from Marresearch-Charged Coupled Device) (Rayonix LLC, Evanston, IL). The HKL2000 program package (HKL Research, Inc., Charlottesville, VA) (*78*) was used for integration and scaling.

Structure Determination and Refinement

The structure of EcPEP was solved by molecular replacement using the program *Phaser* (University of Cambridge, Department of Haematology, Cambridge Institute for Medical Research, Cambridge, England) (*79*), as part of the X-ray crystallography software suite CCP4 (STFC Daresbury Laboratory, Daresbury, Warrington, England) (*80*). The products bound crystal structure of EcPFK (1PFK) (*55*) was used as the model for molecular replacement. PHENIX (Lawrence Berkeley National Laboratory, Berkeley, CA) (*81*) was used for rigid body refinement of the structure. Manual modifications and fittings were performed using COOT (York Structural Biology Laboratory, University of York, Heslington, York, England) (*82*). After each manual refinement using COOT, the structure was again refined by PHENIX until the R-factors converged. The stereochemical quality of the final EcPFK model was verified by MolProbity (Department of Biochemistry, Duke University, Durham, NC) (*83*).

Data collection and refinement statistics for the crystal structure of PEP bound EcPFK are found in table 2-1.

Data Set	PEP bound EcPFK
Unit cell (Å)	a=78
	b=78
	c=114
	β=105
Space group	P 1 2_1 1
Number of molecules per asymmetric unit (Z)	4 monomers
Resolution (Å)	31-2.8
Refinement	
Resolution (Å)	31-2.8
Reflections (working/free)	32569(1654)
R (%)	21.42
Rfree(%)	30.28
Number of overall atoms	9836
Number of protein atoms	9593
Number of ligand atoms	40
Number of water atoms	203
Average *B* factor (Å2)	44.0
Average *B* factor for water molecules (Å2)	41.04
Rmsd Bond length (Å)	0.007
Rmsd Bond angles (degrees)	0.957
Ramachandran statistics	
Most favored	83.48
Allowed	9.30

Table 2-1: Data Collection and Refinement Statistics for PEP bound EcPFK

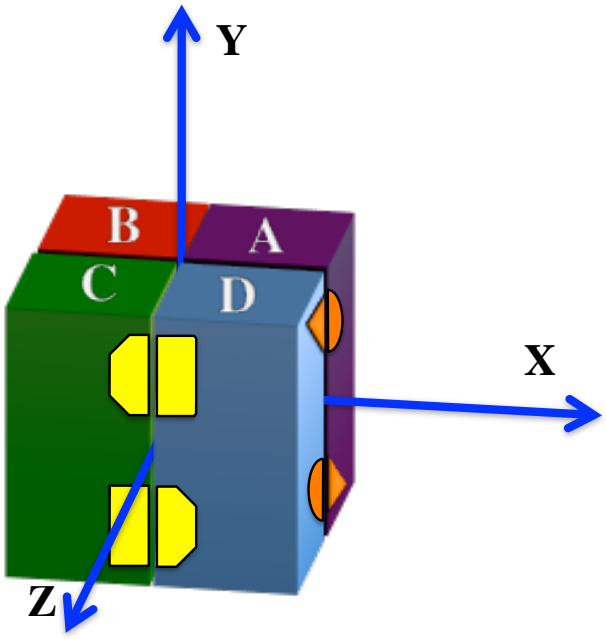

Figure 2-2: Representation of the four homo tetramers of EcPFK. Each monomer is represented by a different color and a different letter. The allosteric sites, yellow octagons, are located on the *yz*-plane and the catalytic sites, orange squares, are located on the *xy*-plane.

Subunit	B	C	D
A	0.58 Å	0.37 Å	0.59 Å
B		0.58 Å	0.43 Å
C			0.62 Å

Table 2-2: The RMSD values between the alpha carbons of each of the PEP bound EcPFK subunits. These values were calculated using UCSF Chimera (*84*).

Results and Discussion

General Structure

The asymmetric unit of EcPEP consists of four subunits that form the native homotetramer. The four allosteric sites lie on the interface residing along the *yz*-plane while the four catalytic sites lie at the interface along the *xy*-plane (Figure 2-2). Since EcPFK and BsPFK are both homotetramers, they can each be described as a dimer of dimers. The dimers will be designated as dimers AB and CD when dividing the tetramer along the *xy*-plane (Figure 2-2). EcPEP has a space group of p 1 2_1 1 and a final resolution of 2.8Å. There are a total of 320 residues represented in this structure. EcPEP has a total of 203 water molecules. There are four PEP molecules identified in EcPEP, one bound to each of the four allosteric sites. The four monomers in the structure differ slightly from each other as evidenced by root-mean-square deviation (RMSD) values between the aligned alpha carbons ranging from 0.37Å to 0.62Å (see Table 2-2 for all RMSD values). Monomers A and C have an RMSD of 0.37Å. Monomers B and D have an RMSD of 0.43Å (Table 2-2). The b-factors for the individual monomers also show small variance but remain quite similar (Figure 2-3). Given the small variances throughout the structure all further results and discussion will be in reference to monomer C unless noted otherwise.

The overall structure of EcPEP is similar to BsPG but more similar to the two previously reported EcPFK structures (*53, 55, 56*). When superimposed, the alpha carbons of EcPEP and BsPG give an RMSD value of 0.80Å.

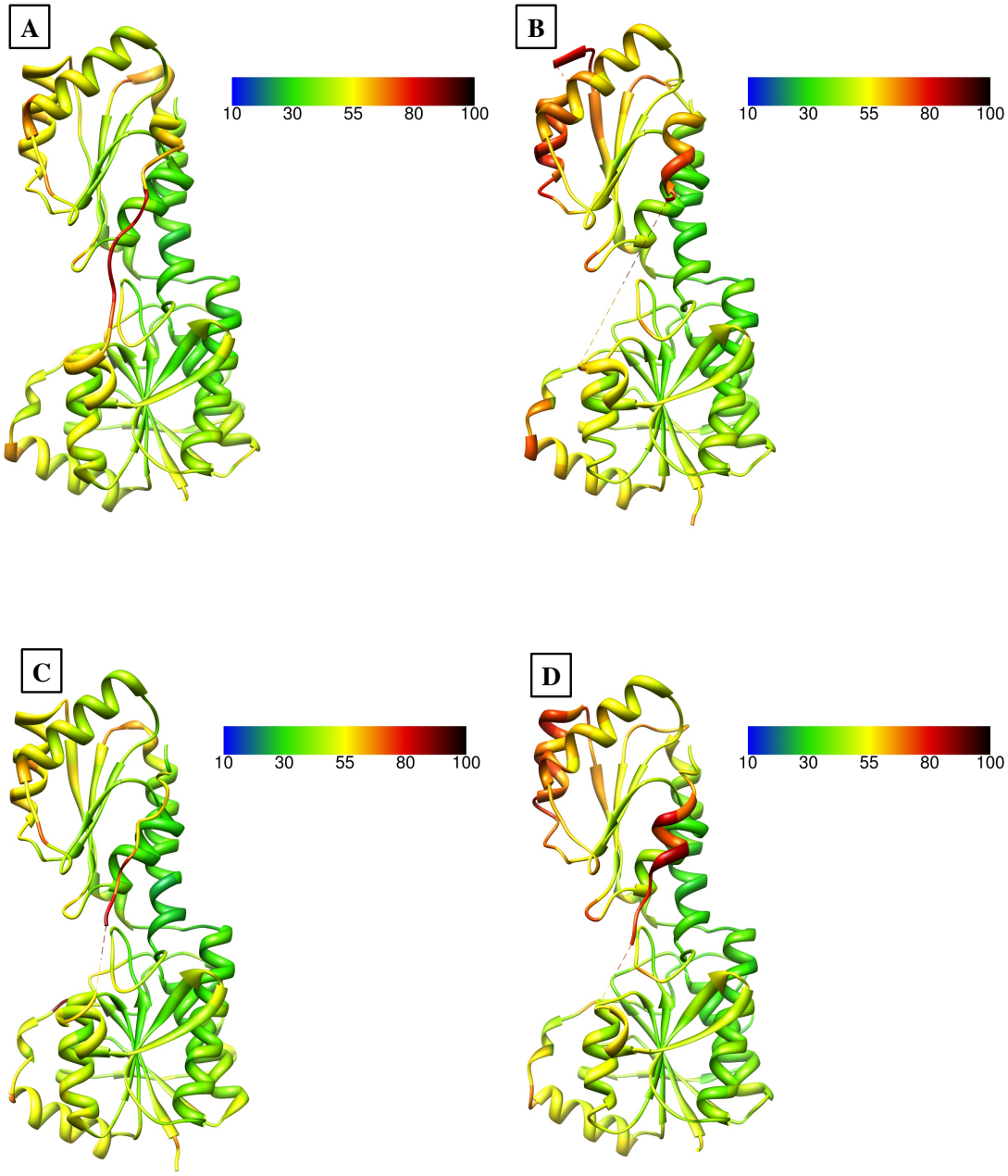

Figure 2-3: Comparison of B-factors between the individual monomers of PEP bound EcPFK. The monomers are designated A, B, C, and D.

When EcPEP is superimposed with EcApo and EcATC the RMSD values are 0.64Å and 0.72Å, respectively (Table 2-3). The larger RMSD value between EcPEP and BsPG is not surprising since the two proteins only share a 55% amino acid sequence identity. The RMSD values are based on the alignment of the alpha carbons between two proteins and therefore inherently related to the extent of sequence identity. These RMSD values further emphasize the fact the EcPFK and BsPFK are distinct proteins and should not be viewed as interchangeable. The remainder this section will focus on the comparison between EcPEP, EcApo, EcATC, and BsPG. Even though BsPG is a different protein, there is value in highlighting the differences between the two inhibitor bound structures, EcPFK and BsPG.

Subunit Interfaces

EcPEP displays a quaternary rotation between dimers AB and CD, about the *z*-axis, similar to that seen in BsPG but to a lesser degree (*53*). UCSF Chimera was used to measure the quaternary rotation (*84*). First the designated AB dimers of the EcPEP structure and a reference EcPFK structure, are superimposed while allowing the CD dimers to be excluded from the calculation. Second, in a separate step the CD dimers are aligned while allowing the AB dimers to rotate freely. Once the CD dimers are aligned the "measure rotation" command is used, with respect to EcPEP in this example, to display the degree of rotation required to align the CD dimers from the resting position where the AB dimers are aligned. For a comparison, the BsPG quaternary rotation relative to BsATC, reported by Evans *et al.* as 7° (*53*), was measured utilizing UCSF Chimera and yields a value of 6.9°. Using EcApo as the reference for the relative positions of the AB and CD dimers, we assessed the rotation of both EcPEP and EcATC. The rotation for EcPEP relative to EcApo is +2.9°. The rotation about the *z*-axis for EcATC relative to EcApo is -2.0° (Table 2-4). This finding suggests that

Structures Compared	RMSD value (Å)
EcPEP – EcApo	0.64
EcPEP – EcADP	0.72
EcPEP – BsPG	0.80

Table 2-3: RMSD values between the crystal structure of the PEP bound EcPFK and the ADP bound structure of EcPFK, the apo structure of EcPFK, and the PG bound structure of BsPFK.

Structures	Rotation	Structures	Rotation
EcPEP vs. EcATC	4.8°±0.1°	BsPG vs. BsATC	6.9°±0.1°
EcPEP vs. EcApo	2.9°±0.1°	BsPG vs. BsApo	5.8°±0.1°
EcApo vs. EcATC	2.0°±0.1°	BsApo vs. BsATC	1.2°±0.1°

Table 2-4: The degree of quaternary structure rotation, between the AB and CD dimers, about the *z*-axis for EcPFK and BsPFK. BsApo is the apo BsPFK structure, PDB entry 3U39.

EcApo does indeed reflect a unique conformation, contrary to the conclusion by Evans *et al. (56).*

The quaternary rotation of BsPG has been attributed to the higher ratio of subunit interface area between individual subunits within the AB/CD dimers along the *yz*-plane (intra-dimers) versus the subunit interface area across within the AD/BC dimers (inter-dimers) along the *xy*-plane (*53*). BsPG shows a intra to inter-dimer interface ratio of 1:0.58 (intra:inter). EcPEP also has an intra to inter-dimer interface ratio of 1:0.58. However, BsApo and EcApo have intra to inter-dimer contact ratios of 1:0.61 and 0.83:1, respectively, (Table 2-5). The data in Table 2-5, shows that EcPEP has an increased intra-dimer subunit interface area of nearly 2-fold and decreased its inter-dimer subunit interfaces by almost 12% with respect to EcApo.

BsPG shows a relatively moderate 14% intra-dimer and 9% inter-dimer subunit interface change compared to BsApo. EcATC has an intra to inter-dimer interface ratio of 1:0.74. Relative to EcApo, EcATC displays an increase in its intra-dimer subunit interface area by almost 2.3-fold and a 1.4-fold increase in its inter-dimer subunit interfaces. The subunit interface comparison shows that PEP has a larger impact on EcPFK than PG has on BsPFK. This finding is somewhat contradictory since EcPEP displays a smaller quaternary structure rotation than the BsPG structure. The data do not indicate whether the difference in the relationship between the change in monomer contact and quaternary structure rotation is a result of different allosteric ligands, different proteins, or a combination thereof.

For each monomer subunit, β-strand I (β-I) lies at the *xy*-interface. BsPG shows β-I for each subunit has moved closer to the interface and form two new hydrogen bonds with the neighboring β-I, relative to the other BsPFK structures (*53*).

Structure	Intra or Inter	Contact Area (Å^2)	Ratio (xy:yz)	Structure	Intra or Inter	Contact Area (Å^2)	Ratio (xy:yz)
EcPEP	intra	1950	1 : 0.58	BsPG	intra	2300	1 : 0.58
	inter	1140			inter	1330	
EcApo	intra	1070	0.83 : 1	BsApo	intra	2010	1 : 0.61
	inter	1290			inter	1220	
EcATC	intra	2450	1 : 0.74	BsATC	intra	1260	0.59 : 1
	inter	1820			inter	2130	

Table 2-5: Intra and inter dimer subunit contact area ratios. The contact area between dimers is given for apo, MgADP bound, and PEP bound structures of EcPFK. The data for apo, MgADP bound, and PG bound BsPFK is listed for comparison.

In BsPG, Thr245 of β-I forms a hydrogen bond with the main chain of the neighboring subunit's β-I. EcPEP does not show any hydrogen bonding between the neighboring β-I. Also, the EcPEP structure does not provide evidence of a notable decrease in distance between the two β-I at the *xy*-interface. It should also be noted that no hydrogen bonding or significant changes in distance occur between neighboring β-I for EcApo and EcATC as well (Figure 2-4). This lack of β-I interaction suggests that EcPFK does not propagate the same structural changes as BsPFK.

Another interface characteristic across the *xy*-plane is the 6-F loop interacting with T70 in BsPG. Here A157 and S159 of the 6-F loop are seen interacting with T70 across the interface (*53*). In EcPFK all three of these positions are serine residues. In the EcPEP structure , S157 and S70 are not interacting with any residues across the *xy*-interface. S159 is primarily seen hydrogen bonding with D12 ($159_{(OH\gamma)}$-$12_{(O\delta)}$) and T66 ($159_{(OH\gamma)}$-$66_{(O)}$) across the subunit interface. The positions of D12 and T66 allow S157 and S159 to maintain their contributions to the helical structure of the carboxy terminal end of α-helix 6 (Figure 2-5). The structural implications of α-helix 6 are further discussed later with the effector binding site. For both EcATC and EcApo, S157 does not interact across the *xy*-interface while S70 is shown hydrogen bonding with S159 of the neighboring monomer. EcATC and EcApo also possess the same D12 and T66 interaction displayed by EcPEP.

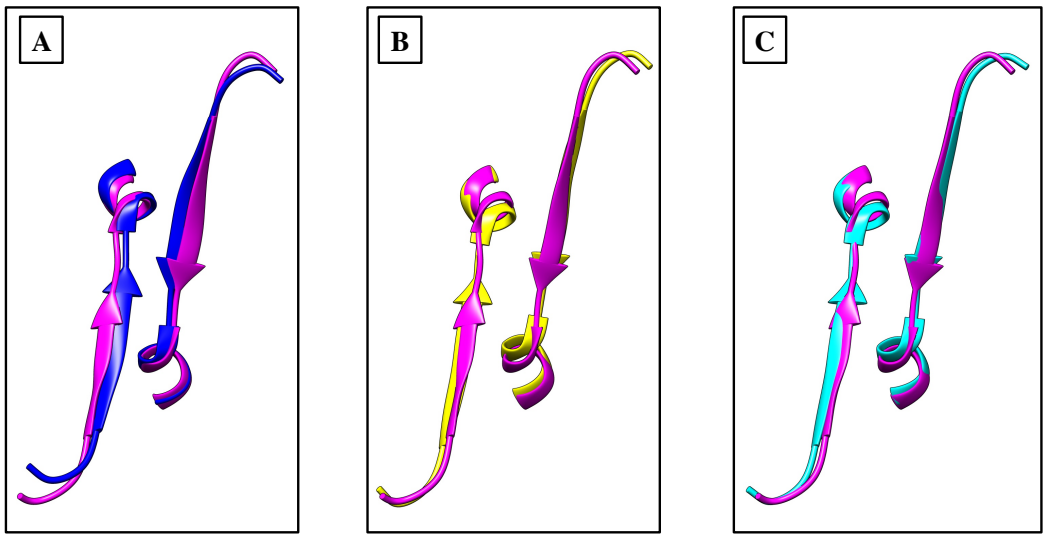

Figure 2-4: The figures above show the positioning of beta strand I from neighboring monomers across the *xy*-interface in EcPEP (purple) aligned with BsPG (dark blue) in box A, EcADP (yellow) in box B, and EcApo (cyan) in box C.

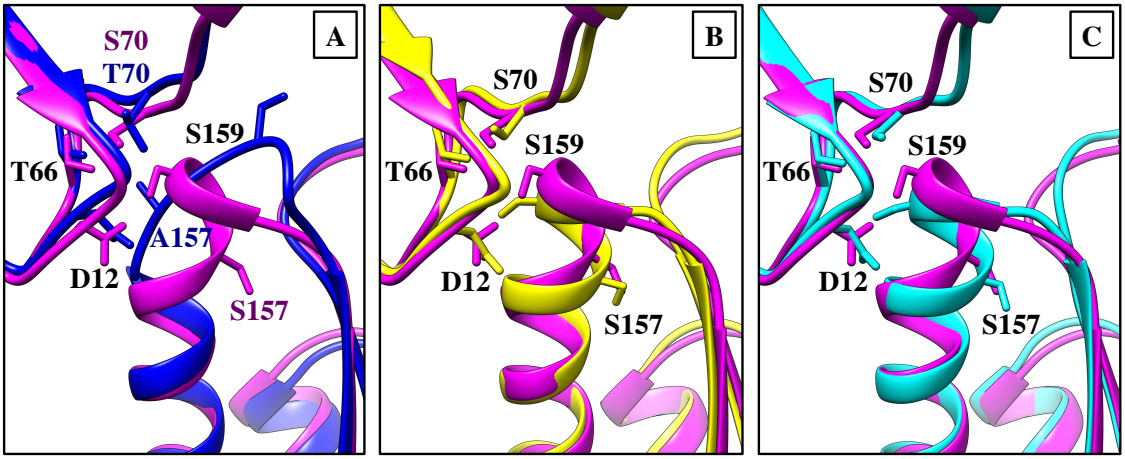

Figure 2-5: The figures above show the positioning of 6-F loop in EcPEP (purple) aligned with BsPG (dark blue) in box A, EcATC (yellow) in box B, and EcApo (cyan) in box C.

Active Site

The BsPG active site was noted by Evans et al. to only have a few changes to the ATP binding site relative to BsATC *(12)*. The R72 side chain forms a salt bridge with E241 across the *yz*-interface, which could potentially leave R72 unavailable for ATP binding interactions (*53*). In EcATC the R72 side chain was reported to be interacting with both the products FBP and ADP (*55*). EcPEP does not show or imply the R72 side chain to be involved in any type of protein interactions. R72 is instead directed towards the solvent. Although the EcApo structure does not have the complete coordinates for the side chain of R72, the backbone and side chain atoms through the γ carbon appear to have adopted a similar position to that of R72 in EcPEP.

A characteristic of BsPG noted by Evans et al. to be critical to BsPFK inhibition is the shift in position of R162 in the F6P binding site with E161 upon the binding of PG *(12)*. The position of E161 in BsPG now allows it to form a salt bridge with R243. E161 is thought to effectively limit the availability of both R243 and R162 which are both important F6P binding residues (*53*). The role of E161 in the mechanism of allosteric inhibition for BsPFK was shown to be minor, at best, by Reinhart et al. (*70*). EcPFK has an asparagine residue at position 161 and not a glutamate. N161 is positioned in the F6P binding site for EcPEP, but would not have the same potential effect of a glutamate at the same position (*67*). N161, in both EcATC and EcApo, is also shown to adopt an extremely similar conformation to that seen in the EcPEP crystal structure. EcPEP does however show R162 to be interacting with the side chain of E241. This interaction is not likely to have a great impact on PEP bound EcPFK since the same interaction also appears in both EcApo and EcATC. R243 along with R252 and E222 were concluded by Evans *et al.* to be positioned in BsPG so

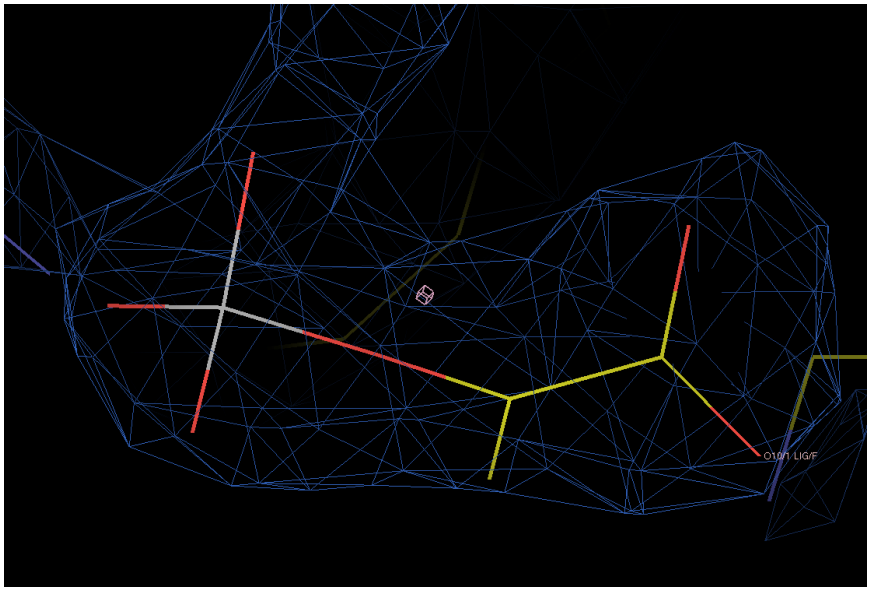

Figure 2-6: **Figure showing the electron density map for PEP bound to wild type E. coli PFK in the EcPEP structure reported in this dissertation. Yellow represents carbon, red represents oxygen, and white represents phosphorus.**

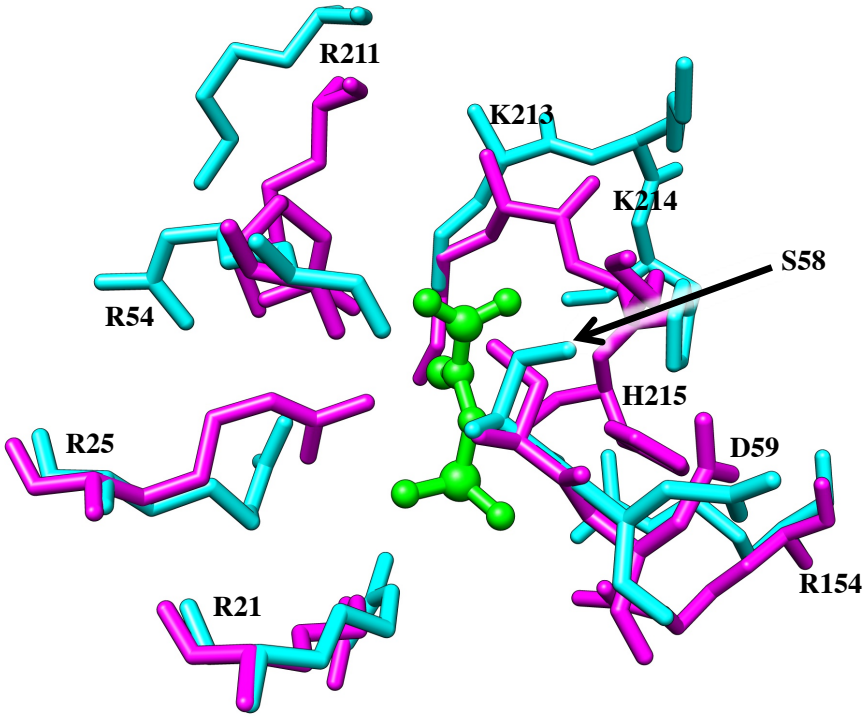

Figure 2-7a: **The overlay of the allosteric effector binding site from EcPEP (purple) aligned with EcApo (cyan). PEP is shown in green.**

that they would clash with F6P when it approached for binding. The same three residues have adopted very similar positions and conformations in EcPEP, although this is once again the case for all three known EcPFK structures. R243, like the aforementioned R72, does not appear to be involved in any notable interactions that could shed light on PEP inhibition.

Allosteric Site:

Figure 2-6 shows the crystal structure with PEP bound to the effector site of EcPFK along with an overlay of the electron density map. This overlay clearly indicates that ligand bound to effector binding site is PEP. The allosteric binding site binds with PEP using 4 residues from one subunit, R21, R25, R54, S58 and two residues from the adjacent subunit across the *yz*-interface, R154 and K214. The phosphate of PEP is directed deep into the binding site and being coordinated by the side chains of residues R21, R25, and R154 (Figure 2-7a). R54 and K214 interact with the carboxylic group oxygens in PEP. S58 appears to interact with the bridging oxygen of PEP. BsPG shows a similar interactions with R21, R25, R154, and K214 (Figure 2-7b). BsPG differs, however, in that it does not show comparable interactions with residues at the 54 and 58 positions, which are valine and glycine, respectively. Instead, BsPG displays R211 interacting with the carboxyl oxygens, while R25 appears to help coordinate the bridging oxygen (*53*). The EcATC structure shows MgADP interacting with all of the same residues that coordinate PEP with a few additional residues (Figure 2-7C). MgADP is also oriented so that the phosphates are directed towards the interior of the enzyme and the adenine moiety is still on the surface of the enzyme. R21, R25, R154, R54, and S58 are all seen interacting with the phosphate oxygens and K214 interact with the hydroxyls of the adenosine moiety. MgADP additionally binds with Y55,

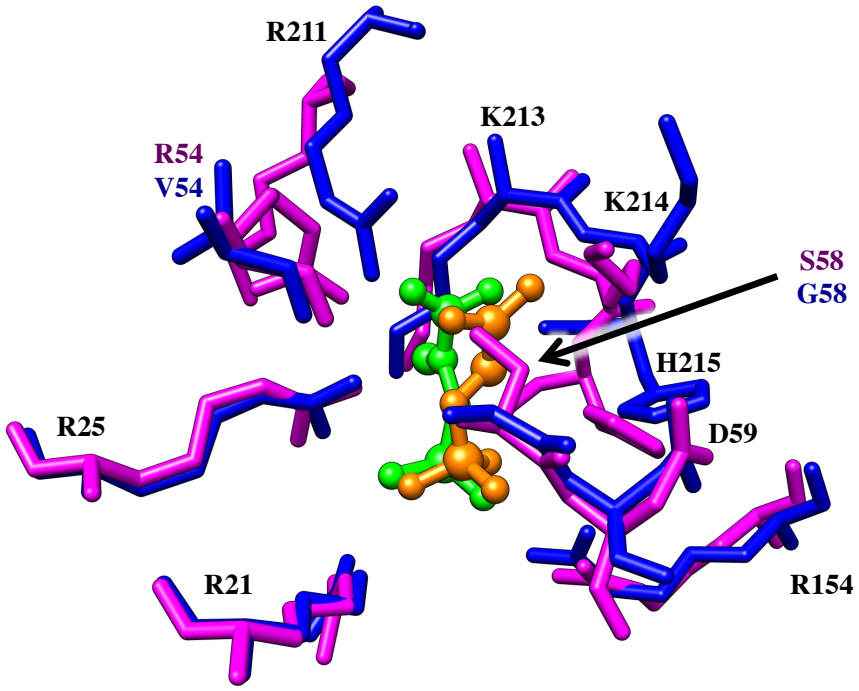

Figure 2-7b: **The overlay of the allosteric effector binding site from EcPEP (purple) aligned with BsPG (dark blue). PEP is shown in green and PG is shown in orange.**

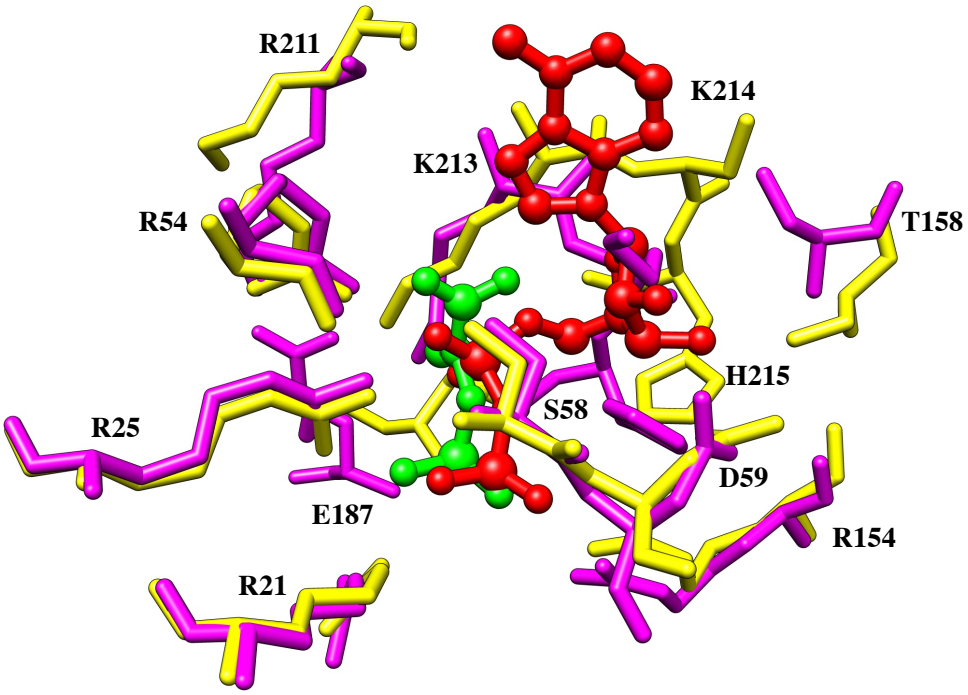

Figure 2-7c: **The overlay of the allosteric effector binding site from EcPEP (purple) aligned with EcATC (yellow). PEP is shown in green and ADP is shown in red.**

D59, and S158. D59 and S158 interact with the hydroxyls of the adenosine moiety while Y55 is thought to base stack with the adenine moiety at the surface of the enzyme.

EcPEP appears to close the allosteric binding site around the PEP molecule. To further characterize allosteric site closure we obtained surface model calculations from the CASTp server (*85*) and viewed them in UCSF Chimera (*84*). Upon examining the CASTp data it is evident that three of the four allosteric sites completely enclose PEP. The fourth allosteric site is completely enclosed except for a small mouth, open towards the solvent, with a calculated molecular surface area of approximately 9.1Å^2. This same type of analysis shows a similar closure of BsPGs allosteric sites, although not a complete closure leaving PG access to solvent. Each allosteric binding site has at least 1 mouth with molecular surface areas averaging approximately 25Å^2 (Table 2-6).

The closure of BsPGs allosteric sites was concluded to arise from the movement of the c-terminal end of α-helix 6 (α-6). α-6 in BsPG loses the helical contributions of residues 157-160 which become part of loop 6-F. The loss of structure to α-6 and lengthening of loop 6-F allows β-strand F (β-F) to shift its position towards the allosteric binding pocket. β-F is hydrogen bonded to β-strand H (β-H) causing β-H to also shift towards the allosteric binding pocket. Finally, loop 8-H hinges at G212 and S216 pushing α-helix 8 (α-8) towards the allosteric binding site(*53*). The loop 8-H residues K211 and H215 make hydrogen bonds across the subunit interface with Y55 and D59, respectively. α-6 in EcPEP does appear tilted at its carboxy-terminal end, relative to EcATC and EcApo, but does not lose its helical conformation. The closure of the allosteric sites indicates once again that the protein and allosteric event captured in the structures of EcPEP and BsPG are very different. The data

Structure (Dimer Pair)	Volume (Å^3)	Pocket Area (Å^2)	# of mouths	Avg Mouth Area (Å^2)	Avg Mouth Circumference (Å)
EcPEP (A-B)	163.8	166.5	1	9.1	10.9
EcPEP (B-A)	150.4	166.8	0	N/A	N/A
EcPEP (C-D)	227.1	231.4	0	N/A	N/A
EcPEP (D-C)	192.8	215.3	0	N/A	N/A
BsPG (A-B)	260.5	235.2	1	19.0	17.2
BsPG (B-A)	283.9	258.9	1	18.7	16.3
BsPG (C-D)	422.3	329.2	2	30.9	22.7
BsPG (D-C)	354.4	299.6	2	25.3	19.3

Table 2-6: The allosteric pocket formation data using CASTp analysis (*85*). For EcPEP, the first subunit listed in each subunit pair (A-B, etc..) contributes residues 21, 25, 54, 55, 57, 58, and 61. The second subunit contributes residues 154, 185, 212, 213, 214, 215, and 319. For BsPG the first listed subunit contributes residues 21, 25, 57, 58, 59, 61, and 62. The second subunit contributes 154, 184, 185, 187, 211, 212, 213, 214, 215, 216, 217, and 319.

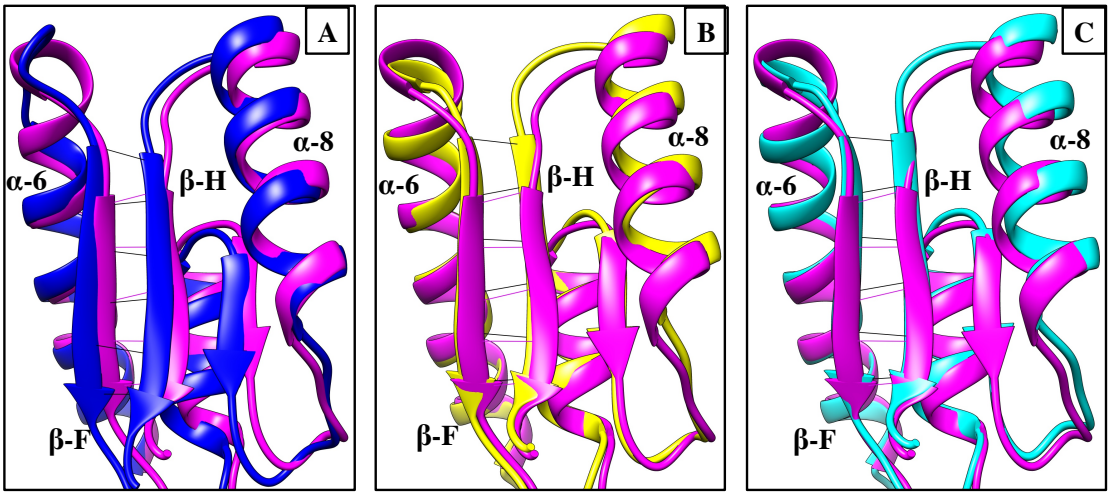

Figure 2-8: The figures above show the interactions between β-strands F and H in EcPEP (purple) aligned with BsPG (dark blue) in box A, EcATC (yellow) in box B, and EcApo (cyan) in box C. Hydrogen bonds for EcPEP are represented in purple and hydrogen bonds for BsPG, EcATC, and EcApo are all represented in black.

presented here cannot distinguish between the contributions of ligand or protein, but they do serve to highlight that the binding of PG to BsPFK and the binding of PEP to EcPFK each produce unique interactions. Instead of loop 6-F stretching, the most amino terminal hydrogen bond between β strand F (β-F) and β strand H (β-H) in the EcATC and EcApo structures is lost, $A216_{(N)}$-$R162_{(O)}$ (Figure 2-8). The result is unzipping of the amino-terminal end of these central strands of the parallel β-sheet GFHI. The separation of β-F and β-H allows the carboxy-terminal end of α-6 to predominantly maintain its helical structure and for α-8 to shift towards the allosteric binding site. This action leaves α-6 and β-F relatively unmoved compared to EcApo and EcADP. The unzipping is stabilized by the hydrogen bond formation between the side chains of K213 and E187, within the same monomer. K213 appears to stabilizing a-13 helix, via E187 interaction, in the EcATC structure. K213 side chain interactions are unclear in EcApo since its side chain is unresolved. For both EcATC and EcApo, the E187 side chain is also hydrogen bonding with I217. EcApo shows an additional interaction between the side chains of E187 and R153.

Conclusion

The 2-state Model has been used to characterize the previously known crystal structures of EcPFK and BsPFK (*52-56*). Not only has EcATC been characterized as the R-State enzyme but also EcApo (*55, 56*). Thermodynamic linkage analysis, presented in chapter 1, shows that the disproportionation reaction represents a much more accurate depiction of the species of enzymes discussed in this dissertation. The disproportionation reaction describes the equilibrium between the two binary complexes, i.e. the enzyme bound to substrate (EA) or allosteric effector (XE), on one side of the equilibrium and on the other

side is the apo enzyme (E) and the ternary complex (XEA), i.e. where both substrate and allosteric ligand are bound. When accounting for the disproportionation equilibrium, the known crystal structures of EcPFK can be identified as a specific species and characterized independently of the other species. Given the disproportionation equilibrium, EcPEP is the only known crystal structure of an EcPFK binary complex. EcATC represents the activated ternary complex while EcApo represents the unbound enzyme.

In this chapter we have shown that BsPG is, structurally, very different from EcPEP. The differences between BsPG and EcPEP should not be a surprise since BsPFK and EcPFK are different proteins. Though these two bacterial PFKs share 55% amino acid identity, they also have markedly different kinetics and thermodynamic parameters (*17, 62, 69, 71*). The differences BsPG and EcPEP are largely due to the difference in amino acid sequences, but it should not be forgotten that PG is an analog of the natural allosteric inhibitor for both enzymes.

Thermodynamic linkage analysis provides for the identification of another difference between EcPFK and BsPFK, the component contributions of ΔG_{ax}. Since Q_{ax} is an equilibrium constant, we can use it to calculate the free energy of the coupling between A and X. For allosteric inhibition, Q_{ax} is less than 1 and is ΔG_{ax} positive. Allosteric activation yields a Q_{ax} value greater than 1 and a negative ΔG_{ax}. By examining the temperature dependencies of coupling for BsPFK and EcPFK in van't Hoff analyses, equation 2-1 can be utilized to determine the enthalpic and entropic contributions to ΔG_{ax} (Equation 2-1) (*86*).

When ΔH and ΔS have the same sign, equation 2-1 states that ΔH_{ax} and $T\Delta S_{ax}$ oppose one another. If ΔG_{ax} retains the sign of ΔH_{ax} then it is enthalpically dominated. Oppositely, when ΔG_{ax} retains the sign of $T\Delta S_{ax}$ then ΔG_{ax} is entropically dominated.

$$\Delta G_{ax} = -RT ln Q_{ax} = \Delta H_{ax} - T\Delta S_{ax}$$

<u>Equation 2-1:</u> This equation describes the relationship between free energy of coupling (G_{ax}), the enthalpy of coupling (H_{ax}), the entropy of coupling (S_{ax}), and the coupling quotient (Q_{ax}) (*86*). Note that ΔG_{ax} is a standard state free energy ($\Delta G°$) and that we have deviated from the standard notation.

When previously studied, ΔG_{ax} for EcPFK was shown to be enthalpically (ΔH_{ax}) dominated with respect to both allosteric ligands, MgADP and PEP (*18, 69*). The same type of study has shown that BsPFK is dominated by its entropic component ($T\Delta S_{ax}$) for both allosteric ligands (*17, 70*). When considering the thermodynamic origins of allosteric coupling along with all of the data presented in this publication, the use of BsPG as a substitute structure for EcPEP is fundamentally wrong. To properly investigate the allosteric coupling of EcPFK or BsPFK, all of the enzymatic states represented in the disproportionation equilibrium must be considered. In this publication we reported the crystal structure of EcPEP. The EcPEP structure represents the inhibitor bound binary complex of EcPFK and is not a representation of the allosteric coupling between F6P and PEP. The structure of the ternary complex of EcPFK, PEP, and F6P is still needed in order to have a physical representation of the allosteric coupling between F6P and PEP.

3. ANALOGS AND MUTANTS

Introduction

Phosphofructokinase from *Escherichia coli* (EcPFK) is catalytically active as a homotetramer with each monomer comprised of 320 amino acids. The tetramer is approximately 34kDa in size and has four identical catalytic sites and four identical allosteric sites. The four allosteric sites lie on the interface residing along the *yz*-plane while the four catalytic sites lie at the interface along the *xy*-plane (Chapter 2, Figure 2-2). EcPFK catalyzes a phosphoryl transfer from ATP to convert fructose-6-phosphate (F6P) into fructose-1,6-bisphosphate (FBP). EcPFK is inhibited by the glycolytic product phospho-enol-pyruvate (PEP) and activated by its catalytic product MgADP. Both PEP and MgADP result in K-type effects only and, more importantly to the current study, bind to the exact same allosteric site. Not only do the two allosteric effectors use the same site but, as disclosed in chapter 2, PEP clearly utilizes many of the same residues for binding as MgADP. This phenomenon is of great interest due to the fact that the two very different ligands cause markedly different behaviors by EcPFK. PEP causes the K_{ia} for F6P to increase over 100-fold over the uninhibited value, while MgADP causes the F6P K_{ia} to decrease to less than 1/10 the unaffected value. How is EcPFK able to differentiate between two ligands that bind to the same binding site?

Previous studies have proposed the two state model to explain the behavior of EcPFK. The two state model simply suggests that EcPFK exists in an equilibrium between

activated and inhibited conformations of the enzyme. Further, the two state model states that the equilibrium is altered when an allosteric ligand binds to EcPFK, causing the enzyme to favor a particular state depending on the ligand. When using the two state model to explain how EcPFK is able to differentiate between allosteric ligands, the need arises for the identification of the "triggers" for such transitions. The first structure suggested to embody, at least in part, a component of the two state model came in the form of activator bound ternary complex of EcPFK (EcATC) (*55*). EcATC possesses the products, fructose-1,6-bis-phosphate (FBP) and MgADP, bound to the catalytic site and MgADP bound to the allosteric site.

With the first crystal structure of EcATC published, the residues seen interacting with MgADP in the allosteric site became the focus of mutation studies (*55, 87*). Fersht et al. performed kinetic studies on EcPFK allosteric site mutations in the presence of PEP and MgGDP, individually. In this allosteric site study, the group concluded that E187 was critical to the control of the equilibrium between the "R" and "T" states. The mutation E187A was reported to cause a reversal of roles for the two allosteric effectors, i.e. MgGDP becomes an inhibitor and PEP an activator (*87*). Effectively, E187 appeared to be the residue controlling the switch between "R" and "T" states. However when this mutation was studied utilizing thermodynamic linkage analysis, it was shown that MgADP and PEP had not switched allosteric roles. Reinhart et al. determined that E187A merely abolishes the allosteric response elicited by MgADP and, like wild type, displays product inhibition caused by excess MgADP (*88*). In another report Reinhart et al. showed that the observed activation of F6P binding, by PEP, is a MgATP dependent phenomenon which only occurs at MgATP concentrations above 25 μM (*89*). The MgATP dependent phenomenon described by

Reinhart et al. is in agreement with previous investigations performed on wild type EcPFK (*18, 74, 90*). Thermodynamic linkage analysis allowed Reinhart et al. to determine that E187 does not have a large impact on the nature of the allosteric effect but is rather a residue that is critical to the magnitude of said effect.

When examining the ability of EcPFK to differentiate between MgADP and PEP, the obvious focus is the interaction between allosteric ligand and the residues in the enzyme's binding site. In comparing the two native allosteric ligands a large difference between them is their size (Figure 3-1). MgADP is a much larger molecule having a molecular formula of $Mg^{2+}C_{10}H_{15}N_5O_{10}P_2$ and a molecular weight of 427.2. PEP has a molecular formula of $C_3H_5O_6P$ and a molecular weight of 168.0. MgADP has many functional groups, including the moieties of adenine, ribose, and pyrophosphate. PEP is a much simpler compound comprised of a central carbon that is bonded to three functional groups. The three groups are a phosphate, methylene, and carboxyl. Even with such a large discrepancy in size PEP and MgADP bind in much the same manner. Reported in chapter 2, the EcPFK crystal structure with PEP bound to the allosteric site (EcPEP) shows PEP bound deep in the allosteric site. The phosphate of PEP is directed towards the interior of the enzyme with the bridging oxygen (the oxygen connecting the phosphate to the 3 carbon chain) coordinated by S58. The remaining phosphate oxygens are coordinated by residues R21, R25, and R154 (Chapter 2 Figure 2-7c). The carboxyl group is seen interacting with R54 and K214. Analysis of the EcATC structure shows MgADP interacting with all of the same residues that coordinate PEP plus a few

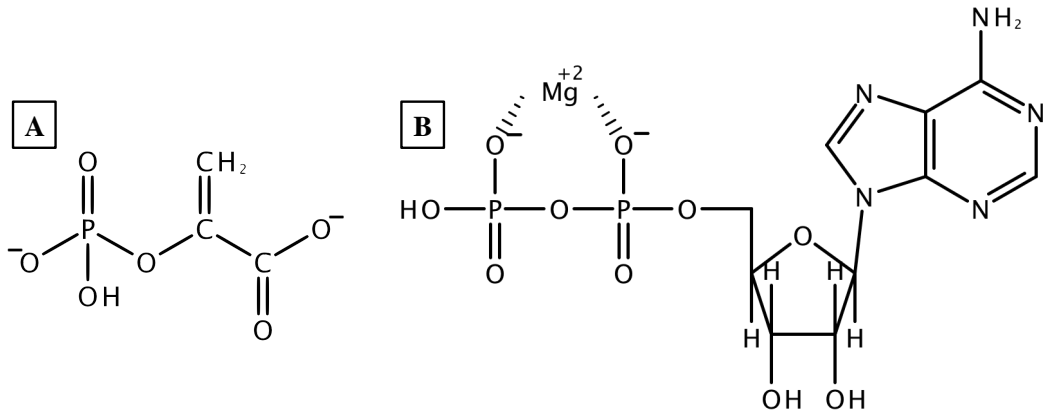

Figure 3-1: The structure of PEP (A) and MgADP (B).

$$K_{1/2} = \frac{K_{ia}^{\circ}\,(K_{ix}^{\circ} + [X])}{K_{ix}^{\circ} + (Q_{ax}[X])}$$

Equation 3-1: Equation representing the K1/2 as a function of effector concentration. Parameters obtained from the fitting of this equation are the coupling quotient (Q_{ax}) the dissociation constant for substrate in the absence of allosteric effector (K_{ia}°) and the dissociation constant of allosteric effector in the absence of substrate (K_{ix}°) (*16*).

additional residues. MgADP is also oriented so that the phosphates are directed towards the interior of the enzyme and the adenine moiety is still on the surface of the enzyme. R21, R25, R154, R54, and S58 are all seen interacting with the phosphate oxygens and K214 interacts with the hydroxyls of the adenine moiety. MgADP additionally binds with Y55, D59, and S158. D59 and S158 interact with the hydroxyls of the adenine moiety while Y55 is thought to base stack with the adenine moiety at the surface of the enzyme (Chapter 2, Figure 2-7c).

Since thermodynamic linkage analysis separately quantifies allostery and ligand binding, in depth studies of the allosteric ligands and allosteric binding sites can help determine the portions of MgADP and/or PEP that are responsible for their individual effects. In this chapter, I present a study of the allosteric ligands of EcPEP in order to define the roles of the functional groups they possess. Comparisons of the natural allosteric ligands and their analogs via thermodynamic linkage analysis, allows the determination as to whether a specific ligand functional group is important to ligand binding, allosteric function, or both.

As stated in chapter one, thermodynamic linkage analysis allows for the determination of dissociation constants for both substrate and effector in the absence (K_{ia}^{o}, K_{ix}^{o}, and K_{iy}^{o} representing substrate, activator, and inhibitor, respectively) and saturating presence (K_{ia}^{∞}, K_{ix}^{∞}, and K_{iy}^{∞}) of each other. These constants are determined by measuring the $K_{1/2}$ of the substrate F6P (A), in saturating MgATP conditions as a function of effector (X or Y, activator or inhibitor, respectively) or effector analog (X' or Y') concentration. By plotting $K_{1/2}$ versus [Y] or [Y'], and fitting to equation (Equation 3-1), the parameters K_{ia}^{o}, K_{iy}^{o}, and Q_{ay} can be obtained (*16*). The free energy of coupling (ΔG_{ay}) between the substrate and effector is then calculated from the Q_{ay} value (Chapter 1, Equation 1-1). ΔG_{ay} is positive

for inhibition, negative for activation, and equal to zero when no allosteric coupling is detected. The dissociation constant of substrate in the absence of allosteric ligand, K_{ia}^{o}, the dissociation constant of allosteric ligand in the absence of substrate, K_{iy}^{o}, and the nature and magnitude of the allosteric event, ΔG_{ay}, are all three critical to the assignment of roles to the ligand functional groups. More specifically, the comparison of these parameters between the native allosteric ligand and a ligand analog allows for molecular difference to be associated with a change in binding, allosteric communication, neither, or both. When the K_{iy}^{o} of an analog effector changes and the ΔG_{ay} does not, relative to the native ligand, the molecular difference is important for ligand binding. In the opposite scenario where only ΔG_{ay} is affected then the molecular difference is important to allostery. Lastly, in a third scenario where both K_{iy}^{o} and ΔG_{ay} are affected then the molecular difference is important to both binding and allostery.

An appropriate follow up to the ligand analog study is the use of thermodynamic linkage analysis to establish the roles of residues on the enzyme that complement the effector analogs. Combining data obtained from the present analog study with information from x-ray crystal structure, amino acids that are in position to interact with the functional groups were identified and examined. Through mutations I attempted to cause EcPFK to exhibit an altered behavior in binding and/or allosteric activity that is comparable to what is seen with the wild type enzyme and the corresponding effector ligand analog. Such a correlation would indeed lend further credence as to the role of ligand functional groups. The ability to replicate analog behavior in mutants would also identify regions of the enzyme that are important in allosteric propagation and binding.

Materials and Methods

All chemical reagents used in buffers for protein purifications, enzymatic assays, and protein crystal development were of analytical grade and purchased from Fisher-Scientific (Hampton, NH), Sigma-Aldrich (St. Louis, MO), Hampton Research (Aliso Viejo, CA), RPI (Natick, MA), MP Biomedicals (Solon, OH). Lyophilized creatine kinase, deoxyribonuclease I, and ammonium sulfate suspensions of aldolase, triosephosphate isomerase, and glycerol-3-phosphate dehydrogenase were purchased from Roche Applied Science (Indianapolis, IN) and Sigma-Aldrich Sigma-Aldrich (St. Louis, MO). All enzymes, except creatine kinase and deoxyribonuclease I, were dialyzed against buffer containing 50 mM EPPS pH 8.0, 10 mM NH_4Cl, 10mM $MgCl_2$, and 0.1 mM EDTA before use. Creatine phosphate, F6P, and PEP were purchased from Sigma-Aldrich. ATP and ADP were obtained from Roche Applied Sciences and/or Sigma-Aldrich. NADH was purchased from RPI. All of the various effector analogs, with the exception of 2-phosphonomethylacrylic acid (PMAA), were purchased from MP Biomedicals and Sigma-Aldrich. PMAA was provided and synthesized by the lab of Dr. Frank M. Raushel, department of chemistry at Texas A&M University (College Station, TX).

Mutagenesis

The plasmid pGDR148 containing the wild type E. coli PFK-1 gene, as described previously (*72*), was used as the starting plasmid for the EcPFK variants created. Site-directed mutagenesis was performed using QuickChange Site-Directed Mutagenesis System from Stratagene (La Jolla, CA). Oligonucleotides were synthesized by Integrated DNA Technologies Inc (Coralville, IA). DNA modifying enzymes were purchased from Promega and New England Biolabs (Ipswich, MA). Qiagen (Hilden, Germany) products were used for

plasmid purifications. XL1Blue cells were obtained from Promega and Stratagene. Two complementary oligonucleotides were used to produce the genes for each of the EcPFK mutants. The template oligonucleotide for each of the pairs of complementary oligonucleotides is shown below. The underlined bases designate the codon for the alternate amino acid that replaced the specific residue indicated.

S58A: GACCGTTACAGCGTGGCGGACATGATCAACCGT

S58C: GACCGTTACAGCGTGTGTGACATGATCAACCGT

S58D: CTAGACCGTTACAGCGTGGATGACATGATCAACCGT

S58N: CTAGACCGTTACAGCGTGAATGACATGATCAACCGTGGC

S58K: CAGCTAGACCGTTACAGCGTGAAAGACATGATCAACCGTGGC

The resulting sequences were verified via DNA sequencing at the Gene Technology Laboratory at Texas A&M University.

Wild-type EcPFK and all of the mutant proteins were expressed from the pGDR148 plasmid which was transformed into competent RL257 cells (MQ ΔpfkB :: FRT ΔpfkB:: ΔpfkA, MQ is a *lac*+ laqiq derivation of MC4100), a PFK-1 and PFK-2 deficient strain (*73*). Once transformed into RL257, the EcPFK producing cells were stored at -80 ºC in a glycerol solution consisting of 50% glycerol, 50 mM TRIS HCl pH 7.5, 5 mM $MgCl_2$, and 0.1 mM EDTA.

Protein Expression and Purification

LB agar plates containing 0.02 mg/ml chloramphenicol were streaked using the appropriate glycerol stock, and grown for 12 hours at 37 ºC. Isolated colonies were then used to inoculate cultures comprising 5 ml of LB and 0.02 mg/ml chloramphenicol and were allowed to grow over night at 37 ºC. Next, Fernbach flasks containing 1.5 L of LB media and

0.02 mg/ml of chloramphenicol were inoculated with 1.5 ml of the overnight culture. The 1.5 L cultures where grown while agitating at 37 ºC for approximately 3 hours, or until the culture reached an OD600 of 0.6. The 1.5 L culture was then induced with 2 mM Isopropyl β-D-1-thiogalactopyranoside (IPTG). Once induced the 1.5 L culture was allowed to grow for an additional 5 hours, or until the culture reaches an OD600 of 1.2. The cells of the 1.5 L culture were then harvested by centrifugation at 4,000 RPM using a Beckman Model J-6B centrifuge. The resulting cell pellet was then stored at -80 ºC.

Wild type and variant EcPFK was purified according to the methods of Johnson et al. with modifications (*74*). The frozen cells were resuspended in 50 mL of TRIS Purification Buffer (50 mM Tris-HCl pH 7.5, 5 mM $MgCl_2$ and 0.1 mM EDTA). Cells were lysed by sonication using a Sonic Dismembrator Model 550 (Fisher Scientific). The sonication protocol consisted of fifteen-second pulses followed by a one-minute rest period to allow the cells to cool. A total sonication time of 8 minutes was used. The crude lysate was clarified by centrifugation at 12,000 RPM for 60 minutes in a Beckman J2-21 centrifuge. The pellet was discarded.The supernatant was incubated in the presence of deoxyribonuclease I at 37 °C for 15 minutes and then centrifuged for 60 minutes. The supernatant containing EcPFK was then diluted to 120 ml using Buffer A (50 mM Tris-HCl pH 7.5, 5 mM $MgCl_2$, 0.1 mM EDTA, and 100 mM NaCl). The 120 ml supernatant containing EcPFK was then loaded onto a column containing a 40 ml bed volume of Mimetic Blue 1 agarose resin, from Prometic Biosciences (Rockville, MD), equilibrated with Buffer A. The supernatant was loaded onto the column at a rate of 2 ml/min. After the supernatant was loaded any unbound protein and/debris was washed from the column using 800 to 1000 mL of Buffer A, or until the pass through from the column had an absorbance of approximately 0.012 at 280 nm. EcPFK was

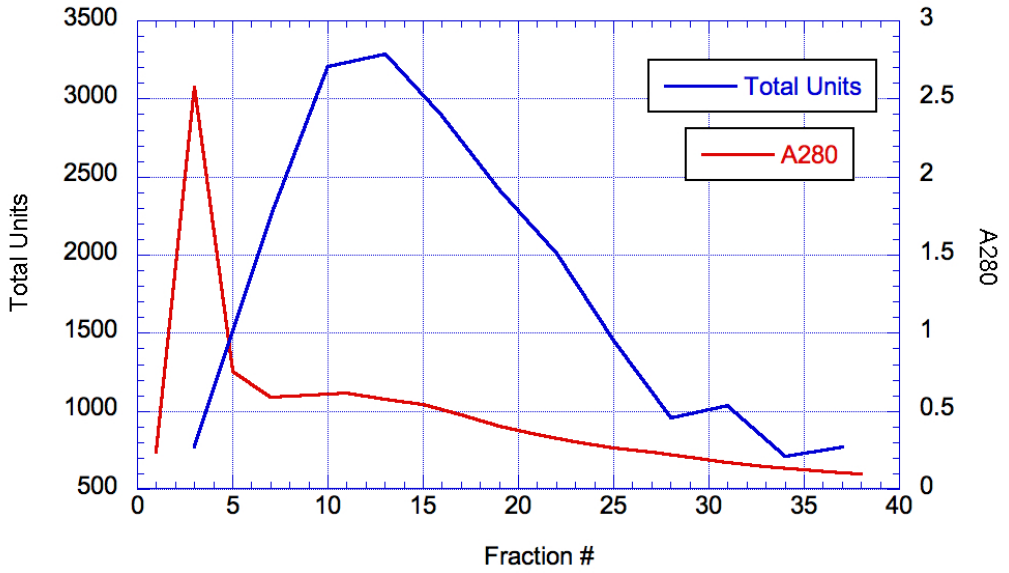

Figure 3-2: Plot of the total units (calculated from maximal activity assays) versus absorption at 280 nm for fractions of EcPFK during the purification process.

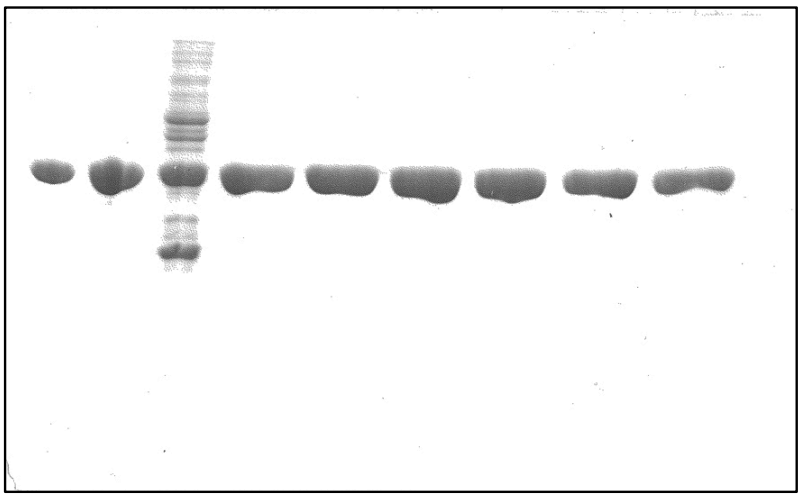

Figure 3-3: SDS-PAGE gel from purification process. Lanes from left to right: EcPFK standard, final sample, crude, fraction #7, fraction #10, fraction #13, fraction #16, fraction #19, fraction #22.

then eluted using a gradient of Buffer A and Buffer B (50 mM Tris-HCl pH 7.5, 5 mM $MgCl_2$, 0.1 mM EDTA, and 2.5 M NaCl) over 200 ml. Fractions were collected in 10 ml increments and checked for PFK maximal activity and A280 reading (Figure 3-2). The fractions having enzymatic activity and low contamination were pooled together as one sample. The pooled sample was then dialyzed against TRIS Purification Buffer and concentrated using Amicon Ultra-15 (100K). The concentrated sample was then dialyzed against EPPS storage buffer (50 mM EPPS pH 8.0, 10 mM NH_4Cl, 10 mM $MgCl_2$, and 0.1 mM EDTA). SDS-PAGE was performed and used to check the EcPFK purity (Figure 3-3). Protein concentrations were determined using the BCA protein assay reagent (*75*). Absorbance readings using $\varepsilon_{278} = 0.6\ cm^2mg^{-1}$ (*76*) were taken and agreed with BCA determined protein concentrations.

Enzymatic Assays

Activity measurements of EcPFK, and its variants, were accomplished by coupling the oxidation of NADH to the reaction catalyzed by EcPFK. The oxidation of NADH was then monitored via its absorbance at 340 nm. The corresponding rate in the decrease of A_{340} was followed and recorded. See figure 3-4 for a detailed coupling scheme. Enzymatic assays were executed by adding 10 µL of approximately 1.8 µg/mL of EcPFK to 590 µL of assay buffer containing 50 mM EPPS-KOH, pH 8.0, 10 mM NH_4Cl, 10mM $MgCl_2$, 0.1 mM EDTA, 2 mM DTT, 0.2 mM NADH, 250 µg of aldolase, 50 µg of glycerol-3-phosphate dehydrogenase, 5 µg of triosephosphate isomerase. The decrease in A_{340} was then monitored for 4 minutes at 25 ºC. When maximal activity was determined, 3 mM ATP and 5 mM F6P were added to the assay cocktail. In enzyme kinetic experiments measuring the allosteric coupling between F6P and either PEP or MgADP, the concentration of all three

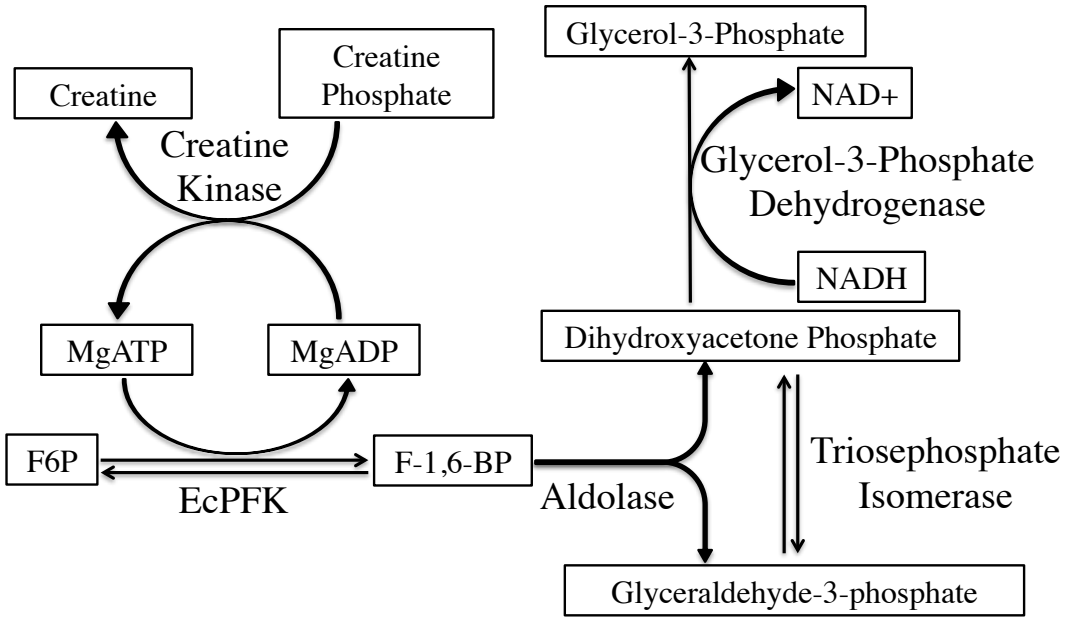

<u>Figure 3-4:</u> A scheme representing the enzyme coupling system used for the assay EcPFK activity. Aldoase, Triosephosphate Isomerase, and Glycerol-3-Phosphate Dehydrogenase are used to couple the oxidation of NADH with the conversion of Fructose-6-phosphate (F6P) to fructose-1,6-bisphosphate (F-1,6-BP). Creatine Kinase, when added, is used for ATP regeneration.

of these ligands are varied correspondingly. Additionally, when measuring the allosteric coupling between F6P and PEP, an MgATP regeneration system is utilized to prevent product inhibition. The MgATP regeneration system was added to the assay cocktail and includes 40 mg/mL creatine kinase and 4 mM phosphocreatine (Figure 3-4). MgADP, being both a reaction product and the allosteric activator of EcPFK, can also compete with PEP for binding at the allosteric sites. When measuring the allosteric coupling between MgADP and F6P, the various additions made of MgADP were added in tandem with equal concentrations MgATP. The equal addition of MgATP helps to negate the product inhibition between MgATP and MgADP in the active site of EcPFK (*18*). The MgADP contamination in the MgATP stock solution was quantified and accounted for all of the MgADP coupling measurements. All activity measurements were performed on Beckman Series 600 spectrophotometers using linear regression to convert the change in absorbance at 340 nm into enzyme activity. One unit (U) of activity is defined as the amount of EcPFK needed to produce 1μmol of fructose 1,6-bisphosphate per minute.

Data Analysis

Allosteric response was determined using thermodynamic linkage analysis (*16*) and applying a single-substrate-single-effector kinetic scheme (discussed in Chapter 1, Figure 1-1). The scheme used assumes that substrate (A) and effector (X) bind at two separate and distinct binding sites on the enzyme (E). The scheme provides for two distinct dissociation constants for each ligand, A or X, found in the absence, K_{ia}° and K_{ix}°, and in the saturating presence, K_{ia}^{∞} and K_{ix}^{∞}, of the other (*16*). The scheme shows the dependence of K_{ia} on [X] (Figure 3-5).

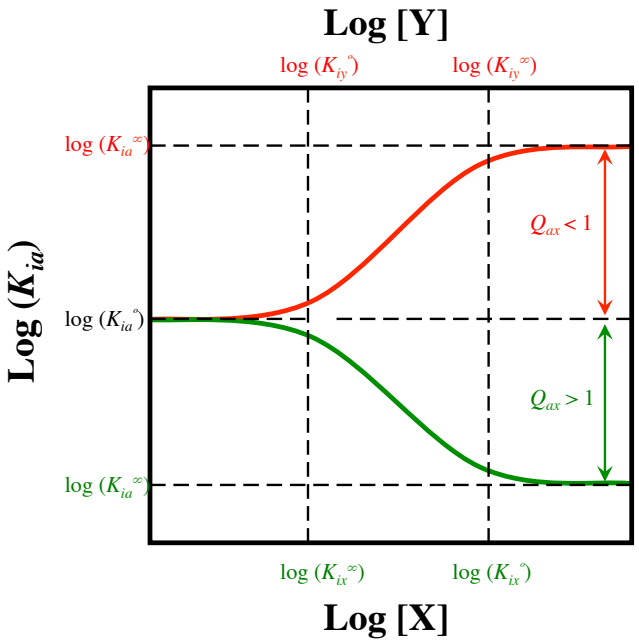

Figure 3-5: Plot of substrate log K1/2 versus the concentration of activator [X] and inhibitor [Y]. The dissociation of a substrate in the absence and saturating presence of effector is represented by the horizontal dashed lines. The vertical dashed lines represent the dissociation constant for the effector in the absence and saturating presence of substrate (*18*).

$$V = \frac{V_{max}[A]^{n_H}}{K_{1/2} + [A]^{n_H}}$$

Equation 3-2: Equation to fit velocity as a function of substrate concentration. V represents initial velocity, V_{max} is maximum velocity, [A] is the concentration of substrate, n_H is the Hill coefficient, and $K_{1/2}$ is the concentration of substrate that results in half the maximal velocity.

$$K_{ix} = K_{ix}^{\circ}\left(\frac{1 + [X']}{K_{ix'}^{\circ}}\right)$$

Equation 3-3: Competitive inhibition equation for determining the binding constant of an allosteric ligand analog in the absence of coupling. Kix is the apparent dissociation constant of the native allosteric ligand, K_{ix}° is the dissociation constant of the native allosteric ligand in the absence of substrate and competitive allosteric ligand analog, [X'] is the concentration of the allosteric ligand analog, and $K_{ix'}^{\circ}$ is the dissociation constant of the allosteric ligand analog.

Ligand	K_{iy}^{0} (mM)	Q_{iy}	ΔG_{ay} (kcal/mol)
PEP	0.41 ± 0.01	0.0111 ± 0.0002	2.66 ± 0.05
PAA	9.4 ± 0.5	0.31 ± 0.01	0.69 ± 0.02
CEPA	55 ± 3	0.29 ± 0.01	0.73 ± 0.02
PG	2.9 ± 0.1	0.021 ± 0.002	2.28 ± 0.22
PMAA	15 ± 1	1	0
MMA	50 ± 10	0.3 ± 0.1	0.7 ± 0.2
P*i*	21 ± 2	0.34 ± 0.01	0.64 ± 0.02

Table 3-1: Comparison of the natural inhibitor, PEP, to the inhibitor analogs that have been examined. Data for PEP, PAA, CEPA, PMAA, MMA, and P*i* were collected at a pH of 8.0 and 25°C. Data for PG is unpublished (*91*) and collected at a pH of 8.0 and 25°C.

Initial velocity rates of EcPFK were plotted as a function of F6P concentrations. The initial velocity data were fit to equation 3-2. K_{ia}^{o}, K_{iy}^{o}, and Q_{ay} were then determined by plotting $K_{1/2}$ versus allosteric effector, and fitting to equation 3-1. In the absence of observable allosteric coupling, the dissociation constant of the allosteric effector analog was determined by competitive inhibition with the native allosteric ligand. When Q_{ay} is equal to zero, equation 3-1 is simplified to equation 3-3.

Results and Discussion

Analogs

Previously unpublished data by Johnson et al. revealed that the K_{iy}^{o} for phosphoglycolate (PG) is increased 10-fold relative to the K_{iy}^{o} for PEP, while the change of ΔG_{ay} for PG is −0.38 kcal/mol from to PEP (Table 3-1, and Figure 3-6) (*91*). Since the experiments were performed with wild type EcPFK, the allosteric and kinetic differences between PG and PEP are due to the differences in molecular and electronic structures between the two ligands. When the molecular structures of PEP and PG are compared, the only difference is the absence of the methylene group in PG (Figure 3-7). These data suggest that the methylene group is involved in both binding and allosteric interactions, with a larger impact on ligand binding.

The next set of analogs focus on the oxygen bridging phosphate to the three carbon chain of PEP, as well as with the methylene group. Phosphonoacetic acid (PPA) and 2-carboxyethylphosphonic acid (CEPA) probe the importance of both the methylene and

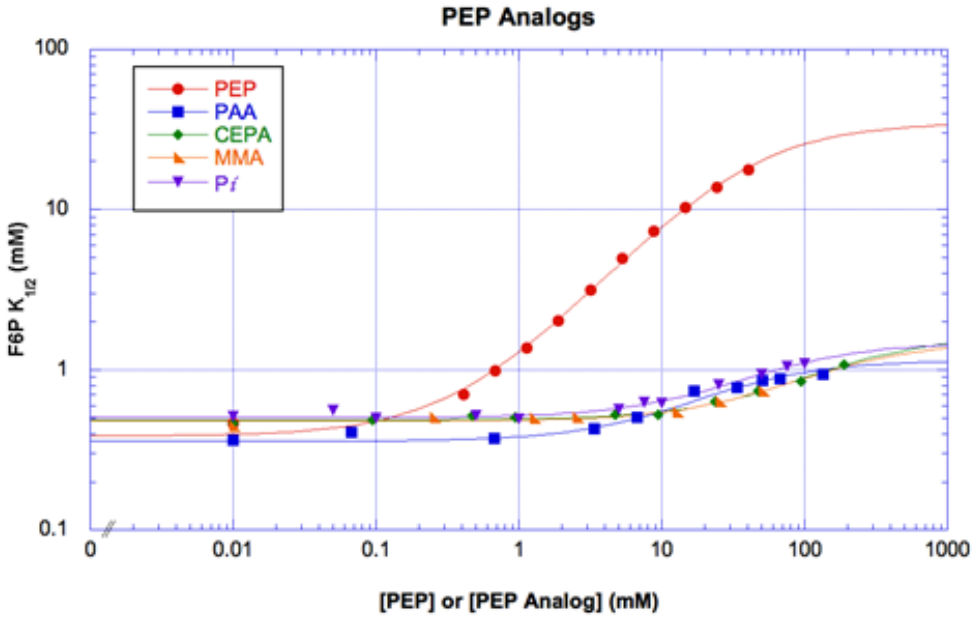

Figure 3-6: F6P $K_{1/2}$ versus [Y] or [Y'] plots. Phospho-enol-pyruvate (PEP, red circles), phosphono acetic acid (PAA, blue squares), carbixyethylphosphonic acid (CEPA, green diamonds), methylmalonic acid (MMA, orange triangles), and inorganic phosphate (P*i*, purple triangles) are all represented. The lines represent the best fit to equation 3-1 for each allosteric ligand.

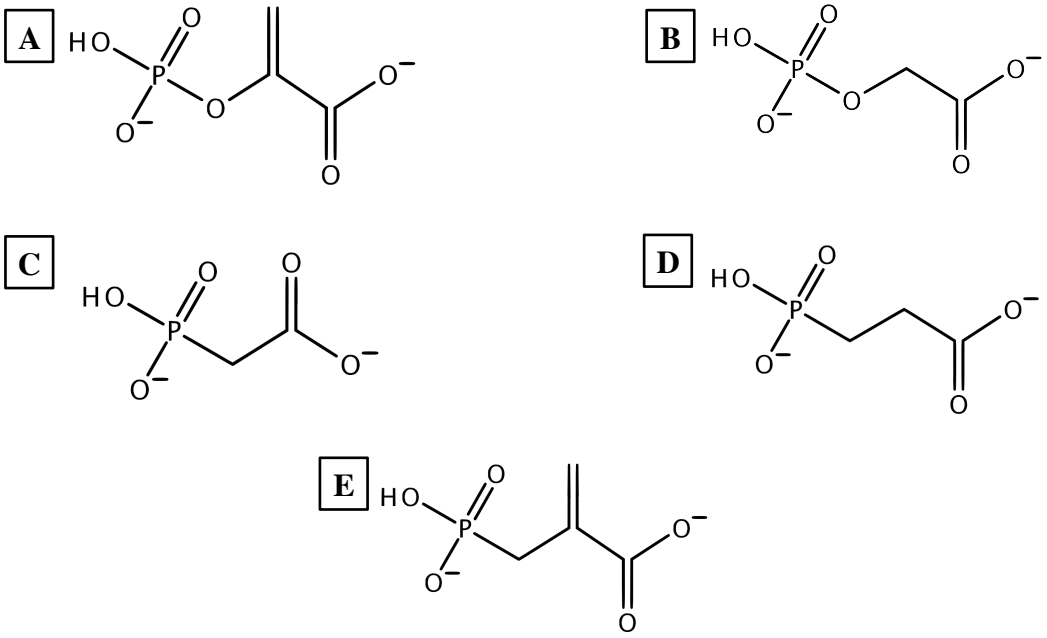

Figure 3-7: Structures of the natural inhibitor, PEP (A), and the inhibitor analogs PG (B), PAA (C), CEPA (D), and PMAA (E).

bridging oxygen present in PEP. PPA, relative to PEP, has a deletion of both the bridging carbon and methylene. The deletion of the bridging oxygen not only removes a potential interaction, but shortens the length of the molecule (Figure 3-7). CEPA also lacks the methylene group. However, CEPA does not have a deletion of the bridging oxygen position but rather a substitution of carbon. The presence of carbon at the position of the bridging oxygen makes the length of the molecule more similar to that of PEP (Figure 3-7). The K_{iy}^{o} of PPA is increased 23-fold (K_{iy}^{o}=9.4 mM) relative to that of PEP (K_{iy}^{o}=0.41 mM). PPA also yields a large change in ΔG_{ay} ($\Delta\Delta G_{ay}$) of −1.97 kcal/mol relative to PEP, a decrease from 2.67 kcal/mol down to 0.69 kcal/mol (Table 3-1, Figure 3-6). The bridging oxygen deletion combined with the methylene deletion in PPA, resulted in substantial changes in binding affinity and allostery. CEPA resulted in a K_{iy}^{o} that is more than 130-fold higher (K_{iy}^{o} =55 mM) than that of PEP and a $\Delta\Delta G_{ay}$ of −1.93 kcal/mol relative to PEP (ΔG_{ay}=0.73kcal/mol) (Table 3-1, Figure 3-6). Replacing the bridging oxygen with carbon instead of deleting it appears to have further decreased ligand affinity without further impact on ΔG_{ay} relative to PPA. Since there are changes to several structural variables with respect to PEP, we can only conclude that the disturbance of both allostery and binding, as seen in PPA, is predominately due to the missing functional groups and not the shortening of the molecules length relative to PEP.

In order to gain more insight into the contributions of the bridging oxygen, phosphonomethylacrylic acid (PMAA) was examined in reference to PEP. PMAA, relative to PEP, has a carbon substitution of the bridging oxygen with no other modifications. PMAA allows for a direct assessment of bridging oxygen to carbon substitution. EcPFK in the presence of PMAA yields a K_{iy}^{o} that is 36-fold larger

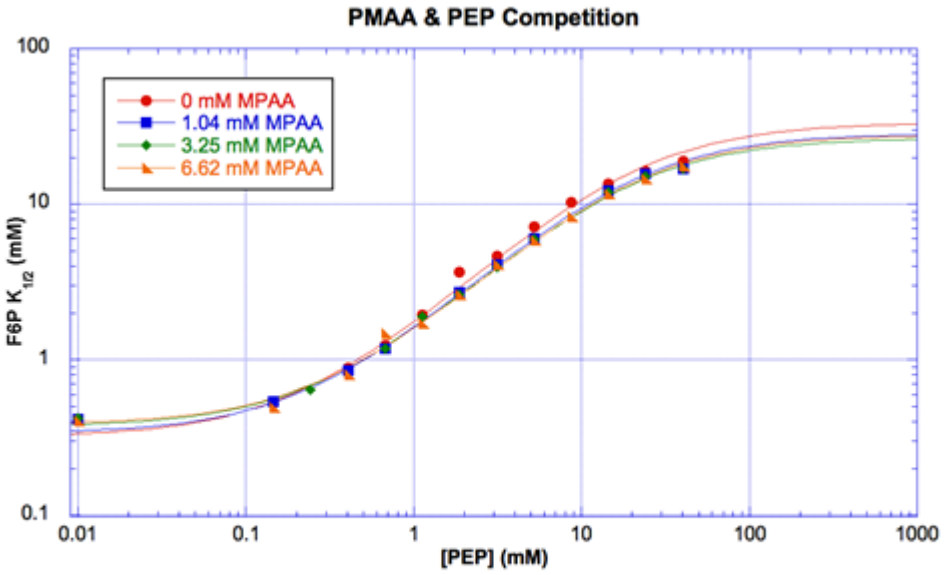

Figure 3-8: Plots of F6P K1/2 versus [PEP] at varying concentrations of 2-phosphonomethylacrylic acid (PMAA). F6P K1/2 at various concentrations of PEP with a PMAA concentration of 0 mM (red circles), 1.04 mM (blue squares), 3.25 mM (green diamonds), and 6.62 mM (orange triangles). The lines represent the best fit to equation 3-1 for F6P $K_{1/2}$ at each concentration of PMAA.

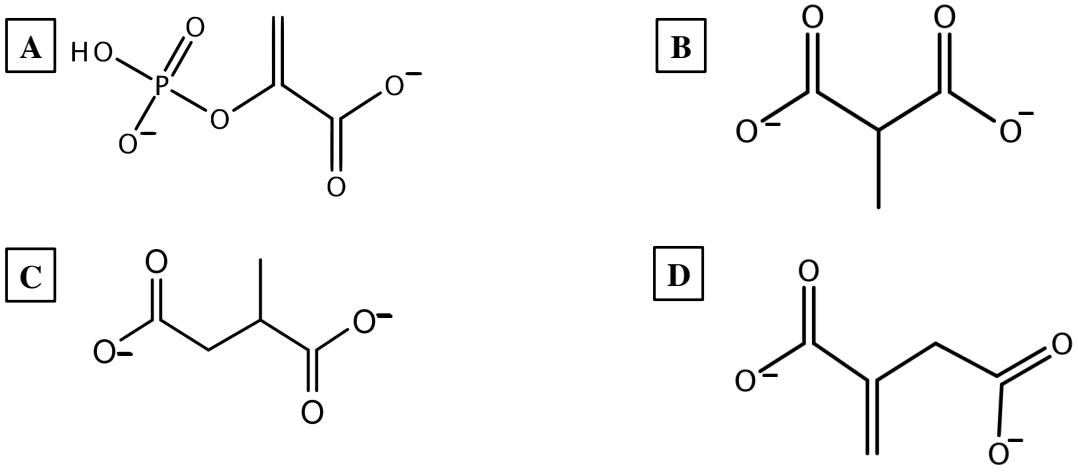

<u>Figure 3-9:</u> Structures of the natural inhibitor, PEP (A), and the inhibitor analogs Methyl-Malonic Acid (B), Methyl-Succinic Acid (C), and Itaconic Acid (D).

(15mM) than PEP with no observable coupling (reference materials and methods section of this chapter for K_{iy}^{o} calculation in the absence of coupling) (Table 3-1, Figure 3-8). This suggests that the bridging oxygen is very important to both ligand binding and allosteric activity. The results displayed by EcPFK in the presence of PMAA also indicate that the replacement oxygen has a much larger impact on allostery. When the PMAA result is considered along side the PG, PPA, and CEPA results, it is clear that the methylene group is primarily involved in ligand binding. The present experiments do not completely explain whether it is the electronic or the steric properties of the oxygen are more important. The experiments do show that PMAA, which is the most structurally similar to PEP, does not bind in a fashion that allows for any detectable coupling.

Next the investigation focused on whether the phosphate on PEP is required for both binding and allostery, and examining the possibility that only the phosphate is required. A series of small non-phosphorylated molecules were studied with wild type EcPFK. A first group of compounds, which replaced the phosphate group of PEP with an additional carboxylate group, comprised methyl-malonic acid, methyl-succinic acid, and itaconic acid (Figure 3-9). Of this group, methyl-malonic acid was the only ligand to render a detectable allosteric effect. The effect was comparable to the effect displayed by CEPA, with a 115-fold increase in the K_{iy}^{o} and a $\Delta\Delta G_{ay}$ of −1.95 kcal/mol, each relative to wild type (Table 3-1). Though, methyl-malonic acid results were similar to CEPA, the error was greatly increased for these experiments and could not be reduced. The first group of ligands intended to look at phosphorylated ligand requirements clearly indicate that phosphate is required for binding and allostery. To test the ability of phosphate alone to elicit allosteric response in EcPFK, inorganic phosphate (P_i) was examined. P_i has a K_{iy}^{o} around 51-fold the

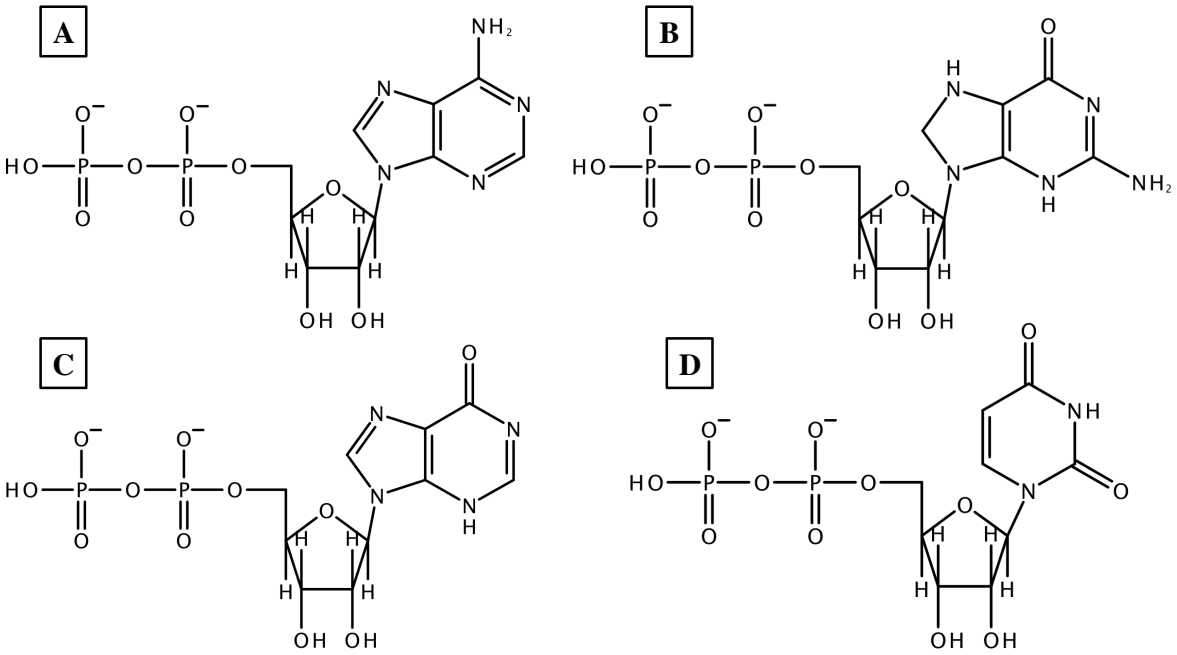

Figure 3-10: Structures of the natural activator, ADP (A), and the activator analogs GDP (B), IDP (C), and UDP (D).

Ligand	K_{ix}^{0} (mM)	Q_{ax}	ΔG_{ix} (kcal/mol)
MgADP	0.073 ± 0.004	11.0 ± 0.2	-1.41 ± 0.03
MgGDP	0.24 ± 0.01	14.2 ± 0.4	-1.57 ± 0.04
MgIDP	0.22 ± 0.01	17.0 ± 0.5	-1.67 ± 0.05
MgUDP	0.85 ± 0.03	13.2 ± 0.3	-1.53 ± 0.03
Mg-dADP	0.027 ± 0.01	11.6 ± 0.1	-1.45 ± 0.01
MgAMP	3.7 ± 0.4	1.8 ± 0.1	-0.35 ± 0.02

Table 3-2: Comparison of the natural activator, MgADP, to the activator analogs that have been examined. All data were collected at a pH of 8.0 and 25°C.

K_{iy}^{o} of PEP. $\Delta\Delta G_{ay}$ is -2.03 kcal/mol relative to PEP and EcPFK (Table 3-1, Figure 3-6). The P_i experiments suggest that phosphate alone is enough to elicit a small inhibitory allosteric effect.

A number of MgADP analogs were also examined for their ability to delineate the contributions of functional groups to allostery and ligand binding. The first functional groups examined were those that belong to the nitrogenous base moiety. The base analogs examined were Mg^{2+} guanosine 5' diphosphate (MgGDP), Mg^{2+} inosine 5' diphosphate (MgIDP), and Mg^{2+} uridine 5' diphosphate (MgUDP) (Figure 3-10). The two analogs consisting of purine rings, MgGDP and MgIDP, examine the importance of the functional groups and their arrangement on the base moiety. Both MgGDP and MgIDP display a K_{ix}^{o} 3-fold higher than MgADP with wild type EcPFK. MgADP has a K_{ix}^{o} of 73 μM while the K_{ix}^{o} for MgGDP and MgIDP are each around 230 μM. The ΔG_{ax} for both MgGDP and MgIDP remains comparable to the natural analog (Table 3-2, Figure 3-11). Experimental results with MgUDP are intended to examine the need for a purine base versus a pyrimidine base. MgUDP also results in a comparable ΔG_{ax} value but exhibits a larger change in K_{ix}^{o} than the two purine analogs. MgUDP has an increased K_{ix}^{o} of approximately 11.6-fold that of MgADP (K_d=850 μM) (Table 3-2, Figure 3-11). Overall, the nitrogenous base moiety appears to only impact ligand binding in a significant manner.

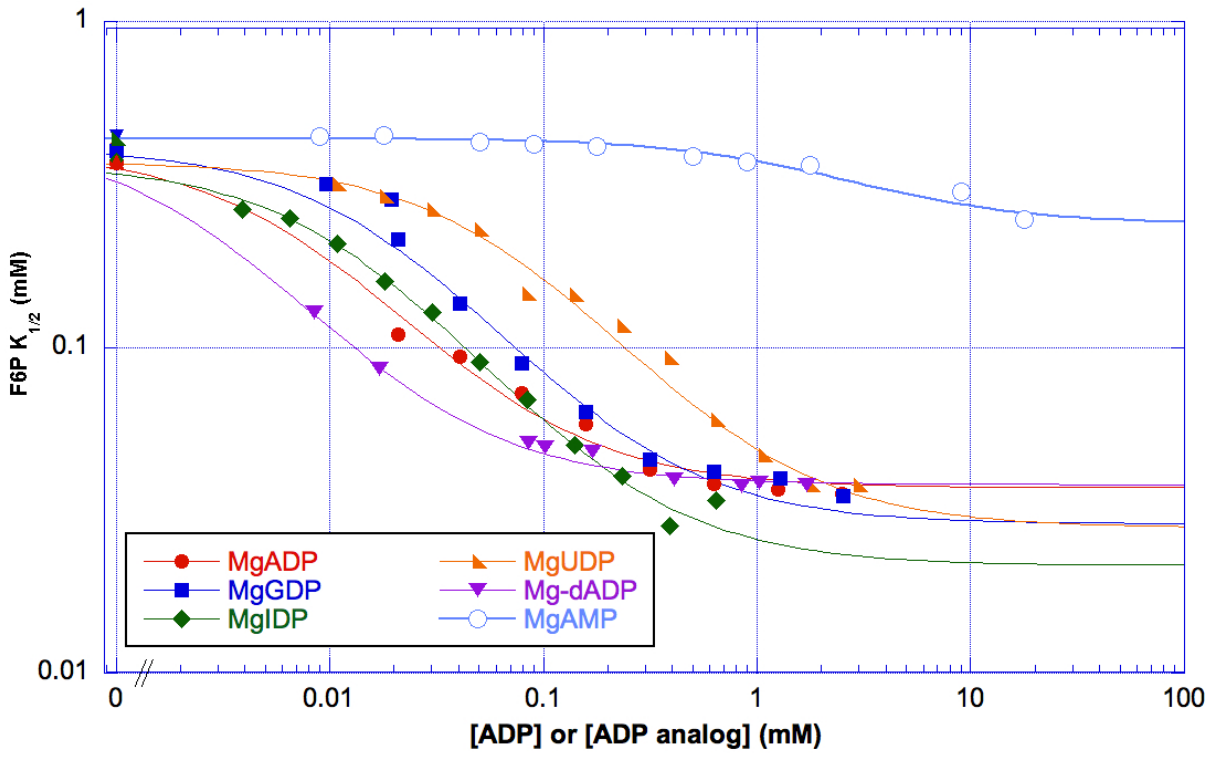

<u>Figure 3-11:</u> F6P $K_{1/2}$ versus [X] or [X'] plots. MgADP (red filled circles), MgGDP (blue squares), MgIDP (green diamonds), MgUDP (orange triangles), MgdADP (purple triangles), and MgAMP (light blue circle outlines) are all represented. The lines represent the best fit to equation 3-1 for each allosteric ligand.

The next group of analogs were selected based on the positioning of MgADP and PEP when they are bound in the effector binding site of EcPFK, as discussed earlier in this chapter and in chapter 2. The analogs Mg 2'-deoxy-adenosine diphosphate (Mg-dADP) and α-β-methylene-adenosine diphosphate (MgAMPCP) were examined (Figure 3-12). The absence of the hydroxyl group at the 2' position of Mg-dADP represents one of the functional groups that could be potentially interacting with the same residues that the methylene and/or carboxylate groups of PEP interact with, i.e. K214 and R54. MgAMPCP possesses a carbon substitution where normally an oxygen bridges α and β phosphates of ADP. Mg-AMPCP represents a change in the structure of MgADP where it would potentially interact with serine 58 of EcPFK. Mg-dADP has a methylene deletion, similar to the PEP analog PG, and retains a highly comparable ΔG_{ax} to that of MgADP. Differing from the homologous PEP analog, Mg-dADP retains a highly comparable K_{ix}^{o}. MgAMPCP results presented the opposite results of Mg-dADP. MgAMPCP did not yield observable binding or coupling. MgAMPCP results indicate that the electronic and/or physical characteristics are so drastically different from MgADP that no binding is observable.

Next, the necessity of phosphate was determined for MgADP. Two analogs were used to examine the necessity of the presence of phosphate as well as specific need of diphosphate. Adenosine represents the removal of all phosphate, while Mg^{2+} adenosine monophosphate (MgAMP) represents the removal of only one phosphate (Figure 3-12). Experiments with adenosine did not yield any observable binding or coupling. The complete removal of phosphate clearly abolishes binding. Unlike adenosine, AMP did exhibit the ability to allosterically activate EcPFK. AMP displayed a K_{ix}^{o} 50-fold higher than that of MgADP.

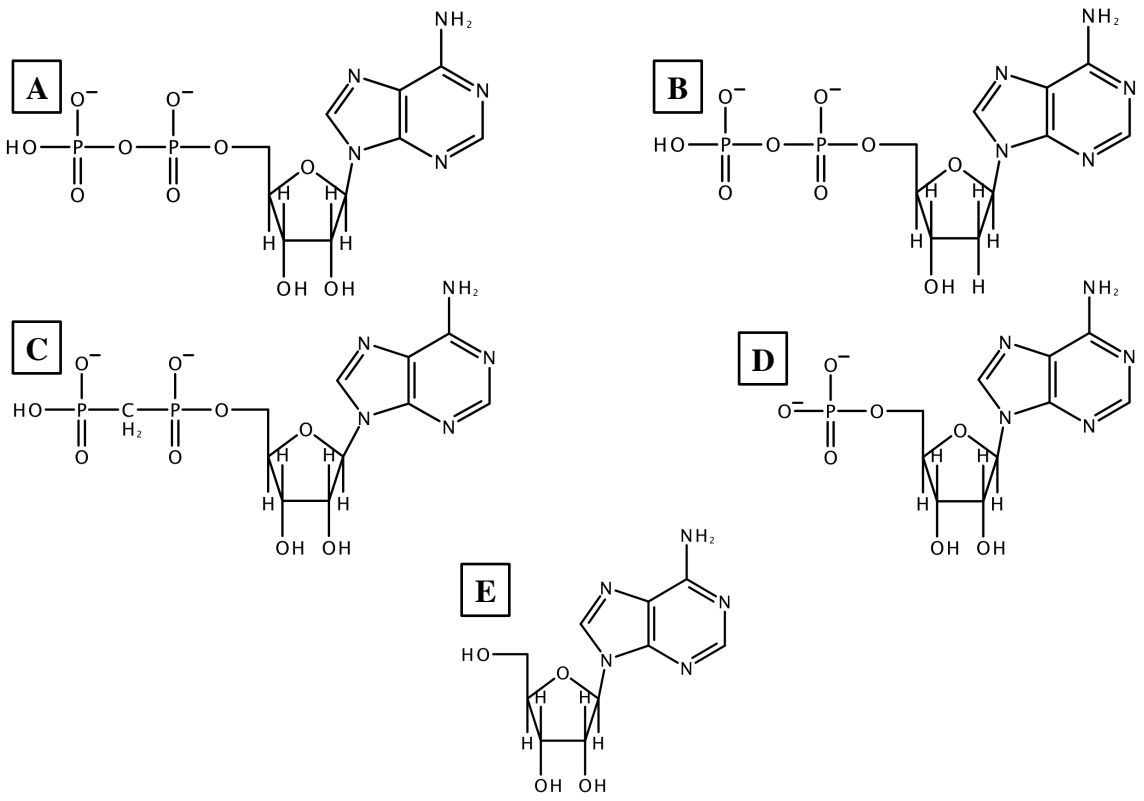

Figure 3-12: Structures of the natural activator, ADP (A), and the activator analogs dADP (B), AMPCP (C), AMP (D), and Adenosine (E).

Allosteric coupling was also greatly impacted, giving ΔΔGax that is +1.07 kcal/mol MgADP (Table 3-2, Figure 3-11). Though adenosine could only imply that phosphate is required for binding, MgAMP allows for the conclusion that the presence of at least monophosphate is necessary for binding and allostery. MgAMP also indicates that the removal of a phosphate from the diphosphate of MgADP significantly impacts both ligand binding and allostery.

Mutations

In examining the results of the analog effector studies for PEP and MgADP, at least one strong conclusion may be drawn. At least one phosphate group is required for the binding of both the inhibiting and activating allosteric effectors. When considering the MgADP analog results alone, the changes to the diphosphate moiety gave the most drastic changes in binding, while changes to the nucleoside moiety had relatively small impacts on binding and allostery. This phosphate centric theme is also seen in the results of the PEP analog experiments. The analog PG, where the methylene group of PEP is deleted, yields minimal impact on binding and allostery. Other PEP analogs that focused on changes involving the phosphate have more substantial impact on binding and allostery. Overall, the analog studies suggest that the portions of the effector molecules closest to the phosphate groups have a greater impact on binding and coupling. The EcPFK activated ternary complex (EcATC) and EcPEP crystal structures strengthen such a conclusion due to the high similarity of positioning seen between MgADP and PEP when bound in the allosteric binding pocket. As discussed previously, the two allosteric effectors align very similarly and use many of the same binding residues in the EcPFK allosteric binding site.

Mutant	K_{ia}^{0} (mM)	K_{ix}^{0} (mM)	Q_{ax}	ΔG_{ax} (kcal/mol)	K_{iy}^{0} (mM)	Q_{iy}	ΔG_{ay} (kcal/mol)
WT	0.408 ± 0.003	0.073 ± 0.004	11.0 ± 0.2	–1.41 ± 0.003	0.41 ± 0.01	0.0111 ± 0.0002	+2.66 ± 0.05
S58A	0.398 ± 0.002	0.25 ± 0.01	11.6 ± 0.3	–1.45 ± 0.06	0.41 ± 0.01	0.04 ± 0.03	+1.9 ± 1.8
S58C	0.442 ± 0.006	0.038 ± 0.001	5.58 ± 0.08	–1.02 ± 0.01	12 ± 1	0.38 ± 0.02	+0.57 ± 0.03
S58D	0.339 ± 0.003	–	1	–	–	1	–
S58N	0.550 ± 0.004	2.8 ± 0.1	3.75 ± 0.07	–0.78 ± 0.1	67 ± 30	0.06 ± 0.3	+1.6 ± 8.3
S58K	9.4 ± 0.2	–	1	–	–	1	–

Table 3-3: Comparison of wild type EcPFK to the position 58 mutant EcPFK that have been examined. All data was collected at a pH of 8.0 and 25°C.

For the reasons mentioned in the previous paragraph, residues were identified that are thought to interact with the portions of the allosteric ligands closest to the phosphate groups. Although there are several residues seen interacting with the phosphate groups of PEP and MgADP, in this study serine 58 was selected for mutation and kinetic study. S58 was selected because when its interactions are compared between EcPEP and EcATC, it can be seen interacting in two different ways. In EcPEP S58 is seen interacting with the bridging oxygen of PEP. In EcATC S58 is primarily seen interacting with the β phosphate of MgADP. Although S58 is still in position to interact with the α-β bridging oxygen of MgADP it does not. This apparent preferential treatment by S58 led to its selection as the focus of the mutation studies for the following experiments.

Using a series of both conservative and non-conservative mutations in the presence of each of the natural effector ligands, serine 58 was examined for its role in the allosteric phenomenon. Alanine, cysteine, aspartate, asparagine, and lysine were all substituted at residue position 58. The first mutation examined was S58A. The alanine substitution is an attempt to disrupt any potential interaction with the bridging oxygen of the allosteric ligands by deleting the hydroxyl group supplied by serine. The K_{iy}^{o} for PEP increased 88-fold, and reduced the coupling free energy by −0.71 kcal/mol from of that seen in wild type EcPFK. Alternatively, experiments with S58A mutation and MgADP, show the K_{ix}^{o} is increased by only 3-fold and displays no change in the allosteric coupling (Table 3-3, Figure 3-13).
In an attempt for a more conservative mutation, the S58C mutant was examined. Cysteine allows for the removal of the serine hydroxyl and replaces it with an alternative sulfhydryl. Results with PEP and S58C reveal a 30-fold increase to K_{iy}^{o} compared to wild type EcPFK. Allosteric coupling is also negatively impacted, with a $\Delta\Delta G_{ay}^{o}$ of −2.09

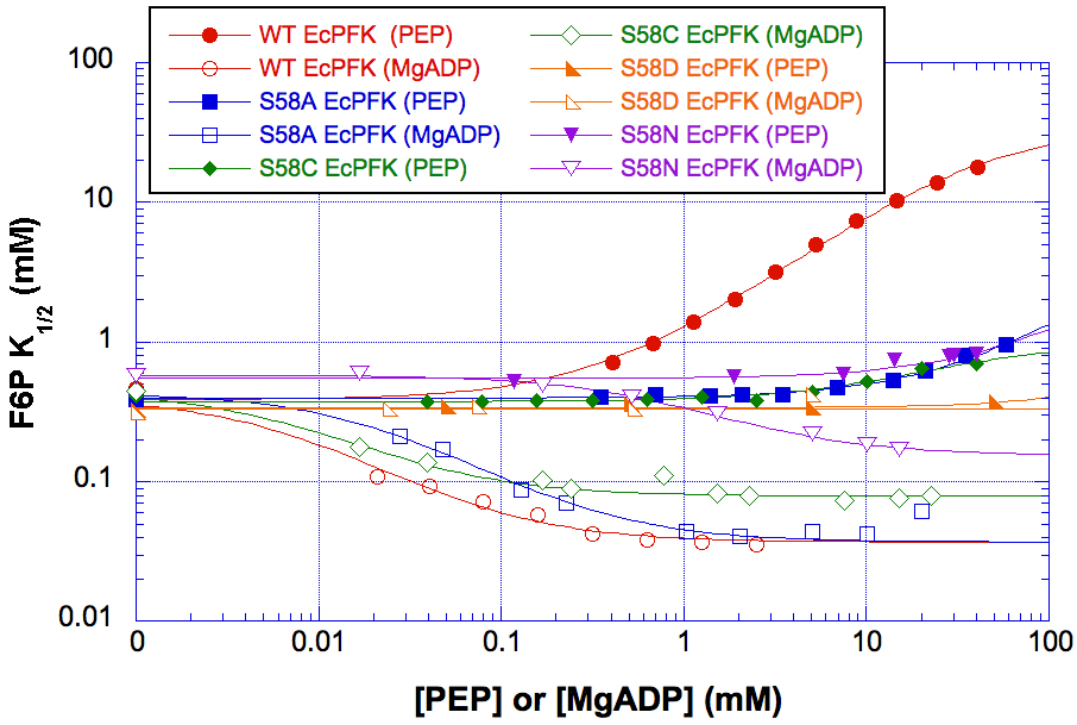

Figure 3-13: **F6P $K_{1/2}$ versus [X] or [Y] plots. Wild Type EcPFK (red circles), S58A (blue squares), S58C (green diamonds), S58D (orange triangles), and S58N (purple triangles) are all represented. PEP points are represented by solid shapes and MgADP is represented by shape outlines. The lines represent the best fit to equation 3-1 for each allosteric ligand.**

kcal/mol, relative to wild type. When MgADP was examined with S58C, the mutant shows a 50% decrease in K_{ix}^{o}. While the S58C mutation has a positive impact on ligand binding, it yields a $\Delta\Delta G_{ax}$ that is +0.40 kcal/mol of that seen in the wild type enzyme. Further probing the type of interaction in which serine 58 is participating, S58N was also selected for study. The substitution to asparagine potentially provides a hydrogen for hydrogen bond interactions. For PEP, S58N displays a large impact on binding and coupling free energy, with a K_{iy}^{o} increased over 160-fold and a $\Delta\Delta G_{ay}$ of −1.00 kcal/mol. Allosteric coupling for MgADP is also dramatically decreased with a difference in coupling free energy of +0.63 kcal/mol from WT EcPFK wild type. While binding of MgADP is significantly impacted, the K_{ix}^{o} is only increased by 38-fold. Both aspartate and lysine mutants yield no observable results with either PEP or MgADP (Table 3-3, Figure 3-13).

Conclusion

Analysis of PPA and CEPA give insight into contributions of both the bridging oxygen and methylene group. Relative to PEP both analogs had a large, but comparable to each other, reduction in allosteric coupling. Binding analysis reveals notable decreases in affinity, but a much larger impact is observed with CEPA. PPA and CEPA are phosphonic acids and have a deletion of the methylene group, relative to PEP. The two analogs differ from one another only in the number of carbons, PPA with two and CEPA with three. The three carbons present give CEPA five bonds from a carboxylic oxygen to a phosphonic oxygen making it a potential better match with PEP (Figure 3-7). Without individually isolating the structural changes in PPA and CEPA, the disturbances of binding or coupling cannot be attributed to any one functional group. Although, we are careful to note that when comparing the results between CEPA and PPA, only affects on ligand binding differed. A decrease in ligand affinity and no change in coupling for CEPA could be a result of an extended freedom of movement for the carboxyl group of the ligand. The double bonded methylene present in PEP can restrict conformations of the ligand. Since methylene is absent in both CEPA and PPA the potential freedom of movement is increased. The third carbon on CEPA could enable more conformations, versus PPA, during a binding event resulting in a reduction of binding affinity.

The individual studies of the bridging oxygen and methylene group were achieved with the use of three additional analogs. Results from PG, methylene minus analog, yield a notable penalty on binding affinity with relatively no change in allosteric coupling. With no other structural difference relative to PEP, the results imply a strong role in ligand binding and little to no role in allosteric coupling for the methylene group. PG analysis also further

supports the explanation given above for differences seen in binding between CEPA and PPA. Change to the bridging oxygen is represented in the analog PMAA. When carbon is substituted for the bridging oxygen, as in PMAA, the observable allosteric coupling is all but destroyed and binding affinity is greatly weakened. The lack of allostery seen with PMAA could be a result steric clash due to the bond angle of carbon at the bridging oxygen position combined with the presence of the methylene double bond. The restriction of conformations due to steric conflicts could potentially result in non-preferred ligand conformations. Given the structural similarity to analogs previously mentioned, PMAA does not necessarily clarify the role of the bridging oxygen but rather further supports the importance of methylene to ligand binding.

Given the positioning of MgADP in the binding pocket the results with MgGDP and MgIDP are not surprising. Modifications of the nitrogenous base moiety resulted in minor impacts on binding and virtually no impact on allosteric activity. When MgADP analogs MgAMPCP results indicate that the electronic and/or physical characteristics are so drastically different from MgADP that no binding is possible.

Like PEP, the necessity of phosphate was determined for MgADP. Two were used to examine the necessity of the presence of phosphate as well as specific need of diphosphate. Adenosine represents the removal of all phosphate, while Mg^{2+} adenosine monophosphate (MgAMP) represents the removal of only one phosphate.

Mutations of residues at position 58 of EcPFK further support the hypothesis of allosteric site interaction with the bridging oxygen. The analysis of PEP with an alanine substitution at position 58 results in a large penalty on both ligand binding and coupling. The detrimental affect on PEP inhibition by S58A shows similarities to observations with the

bridging oxygen analogs. A large affect on both coupling and binding, with a seemingly larger impact on coupling, again suggests the involvement of the of Ser58's hydroxyl group with the bridging oxygen. With a cysteine substitution at the 58 position a notable, but smaller, decrease in ligand affinity observed along with some gain of allosteric coupling, relative to S58A. The relative gain in coupling observed with cysteine could be due to its hydrogen bonding potential of the residue. The potential cysteine as a hydrogen bond donor could also explain S58C's display tighter binding for PEP relative to alanine. We also note that S58C shows a much larger affect on coupling relative to ligand binding. In the case of S58C the 12x increase of K_{iy}^{o}, relative to wild type, is still a much higher affinity than what is seen with any of the bridging oxygen analogs in this study.

Mutations at position 58 also display the ability to differentiate between MgADP and PEP. S58A displays a small decrease in ligand affinity for MgADP while having no impact on MgADP coupling. S58C increases the binding affinity for MgADP and has a small decrease in MgADP coupling. The differential treatment between allosteric activator and inhibitor by the EcPFK mutants demonstrates that activation and inhibition are two separate phenomena. While sharing a ligand binding site certainly suggests that the same residues interacting in one allosteric event are used in the other, our data shows the ability of the enzyme to reassign roles in response to an effector ligands identity.

The mechanism by which EcPFK differentiates between PEP and MgADP as inhibitor and activator, respectively, remains unresolved. Previous data, along with the recently solved PEP bound EcPFK crystal structure, have implicated the interaction of effector site residue Ser58, located in α-helix 6, with the oxygen that bridges phosphate to carbon in PEP. The study of the EcPFK mutant S58A, not only supported the hypothesis of

the existence of this interaction but unexpectedly demonstrated the enzyme's ability to differentiate between the two native ligands . Alanine, which served as essentially a hydroxyl deletion, caused the near disappearance of allosteric inhibition along with a 88x increase in PEP dissociation constant. However, with MgADP, S58A had no affect on allosteric coupling and only a 3x increase in dissociation constant. In the study presented here we analyze additional mutations at the serine 58 postion of EcPFK using thermodynamic linkage analysis.

The ability to differentiate between binding and coupling, via thermodynamic linkage analysis, allows for the assignment of roles to ligand functional groups. Use of linkage analysis with effector ligand analogs, limited to minor modifications, allows for role assignment of the methylene and bridging oxygen of PEP. Methylene appears to primarily make contributions to ligand binding. The bridging oxygen makes a large contribution to allosteric coupling while also making a small contribution to ligand binding. Known structural data of EcPFK suggests that serine 58 is a primary residue of interaction for the bridging oxygen. Mutations at this residue position further support the hypothesis of interaction between Ser58 and bridging oxygen. Ser58 also demonstrates the ability to differentiate between allosteric activator and allosteric inhibitor.

4. CONCLUSION

While there is no doubt that, in a fast paced industry, high throughput design has great merit, there has never been a more obvious need for a thorough understanding of allostery. More specifically, there is a need to better understand the effect of allosteric ligand structure on the characteristics of the resulting allosteric behavior. The relationship between ligand structure and allosteric function is key to the advancement of allosteric based pharmaceutics.

Here I attempt to better understand the relationship between allosteric ligand structure and the resulting allosteric behavior by investigating the roles that functional groups and structure play in the binding affinity and allosteric potency of ligands at the allosteric site of phosphofructokinase from E. coli (EcPFK). EcPFK catalyzes the conversion of fructose-6-phosphate (F6P) into fructose-1,6-bisphosphate (FBP) via phosphoryl transfer from MgATP. EcPFK is allosterically inhibited and activated in the presence of phospho-enol-pyruvate (PEP) and MgADP, respectively. EcPFK also displays very strong homotropic coopertivity towards F6P. Both activator and inhibitor have been shown to bind to the same effector site and result in only K-type effects [8,9]. The fact that both MgADP and PEP bind to the same binding site using a majority of the same residues, makes EcPFK an ideal system for this type of allosteric characterization.

In chapter II, I disclose study of the crystal structure of EcPFK that has been solved with PEP bound to the allosteric binding sites (EcPEP). Over the years, the allosteric

behavior of EcPFK has been speculated to be the result of a shift of its overall structure from an activated state to an inhibited state. A two state type model for allosteric behavior places inherent limits on the variation of characteristics observed for one allosteric ligand versus another. The flipping from one state to another implies that a ligand needs only a minimum structural requirement to stabilize a particular state. Much of this speculation stems from the two published crystal structures of EcPFK and the earlier crystal structures of its homolog, *B. stearothermophilus* (BsPFK) (*52-54*). The known EcPFK publications represent the enzyme in the apo form (EcApo) and the activated ternary complex form (EcATC). The EcATC is bound to FBP and MgADP in the active site, as well as MgADP in the effector site (*55, 56*). Thermodynamic linkage analysis allows the consideration of the enzymatic forms set forth by the disproportionation equilibrium in figure 1. In this scheme EcApo represents "E", EcATC represents one of two possible "XEA". Chapter II presents the first study of EcPEP, the only known binary complex of EcPFK, which represents one of two possible "XE" forms of EcPFK.

Chapter III is a thorough kinetic characterization of the coupling between fructose-6-phosphate (F6P) and allosteric effector analogs. The resulting study suggests the role of functional groups belonging to allosteric ligands. Different effector analogs that vary only slightly from the natural allosteric effectors EcPFK were utilized so that the minor modifications allow for meaningful comparisons of the parameters obtained via thermodynamic linkage analysis with F6P and allosteric ligand. Comparison of dissociation constants (K_d) between the effectors and effector analogs allows for a direct analysis of the affects on binding affinity by the variation present, whereas the comparison of the coupling quotient (Q_{ax}) yields the impact on allosteric response. Chapter III further interrogates the

interactions between ligand and protein via modification of effector site residues. In retrospect, one could reason that the ligand analog study mentioned in the previous paragraph entailed the "mutation" of effector ligands in order to differentiate the functional constituents from their molecular structure. Using the information obtained from the ligand analog study along with what is known about the effector binding site, more conclusions were made about ligand-residue interactions in the effector site. Modification of ligand interacting residues results in altered allosteric response in a manner comparable to those seen with the modified effectors and wild type enzyme.

A fundamental step in hypothesis development is the accurate characterization of the subject. The two state Model has been used to characterize the previously known crystal structures of EcPFK and BsPFK (*52-56*). Not only has EcATC been characterized as the R-State enzyme but also EcApo (*55, 56*). A closer examination of thermodynamic linkage analysis, presented in chapter I, shows that the disproportionation reaction represents a much more accurate depiction of the species of enzymes discussed in this dissertation. The disproportionation reaction describes the equilibrium between the two binary complexes, i.e. the enzyme bound to substrate (EA) or allosteric effector (XE), on one side of the equilibrium and on the other side is the apo enzyme (E) and the ternary complex (XEA), i.e. where both substrate and allosteric ligand are bound. When accounting for the disproportionation equilibrium, the known crystal structures of EcPFK can be identified as a specific species and characterized independently of the other species. Given the disproportionation equilibrium, EcPEP is the only known crystal structure of an EcPFK binary complex. EcATC represents the ternary complex while EcApo represents the unbound enzyme.

Another fundamental step of hypothesis development is the application of concepts, models, and facts. Hypotheses built on such strong foundations lead the way for exceptional research and experiments. A fundamental element of a hypothesis is the remembrance that it is an educated guess. One cannot perpetuate a hypothesis as fact. In this chapter we have shown that BsPG is, structurally, very different from EcPEP. The differences between BsPG and EcPEP should not be a surprise since BsPFK and EcPFK are different proteins. Though these two bacterial PFKs share a 55% amino acid identity, they also have markedly different kinetics and thermodynamic parameters. The differences BsPG and EcPEP are largely due to the difference in amino acid sequences, but it should not be forgotten that PG is an analog of the natural allosteric inhibitor for both enzymes.

Thermodynamic linkage analysis provides for the identification of another difference between EcPFK and BsPFK, the component contributions of ΔG_{ax}. Since Q_{ax} is an equilibrium constant we can use it to calculate the free energy of the coupling between A and X. For allosteric inhibition, Q_{ax} is less than 1 and is ΔG_{ax} positive. Allosteric activation yields a Q_{ax} value greater than 1 and a negative ΔG_{ax}. By examining the temperature dependencies of coupling for BsPFK and EcPFK in van't Hoff analyses, equation 2-1 can be utilized to determine the enthalpic and entropic contributions to ΔG_{ax} (*86*).

Since equation 2-1 states that ΔH_{ax} and $T\Delta S_{ax}$ oppose one another, if ΔG_{ax} retains the sign of ΔH_{ax} then it is considered enthalpically dominated. Oppositely, when ΔG_{ax} retains the sign of $T\Delta S_{ax}$ then ΔG_{ax} is entropically dominated. When previously studied, ΔG_{ax} for EcPFK was shown to be enthalpically (ΔH_{ax}) dominated with respect to both allosteric ligands, MgADP and PEP (*18, 69*). The same type of study has shown that BsPFK is dominated by its entropic component ($T\Delta S_{ax}$) for both allosteric ligands (*17, 70*). When considering the

thermodynamic origins of allosteric coupling along with all of the data presented in this chapter, the use of BsPG as a substitute structure for EcPEP is fundamentally wrong.

Analysis of PPA and CEPA gave insight into contributions of both the bridging oxygen and methylene group. Relative to PEP both analogs had a large, but comparable to each other, reduction in allosteric coupling. Binding analysis reveals notable decreases in affinity, but a much larger impact is observed with CEPA. PPA and CEPA are phosphonic acids and, relative to PEP, have a deletion of the methylene group. The two analogs differ from one another only in the number of carbons, PPA with two and CEPA with three. The three carbons present give CEPA five bonds from a carboxylic oxygen to a phosphonic oxygen making it a potential better match with PEP. Without individually isolating the structural changes in PPA and CEPA, the disturbances of binding or coupling cannot be attributed to any one functional group. Although, we are careful to note that when comparing the results between CEPA and PPA, only affects on ligand binding differed. A decrease in ligand affinity and no change in coupling for CEPA could be a result of an extended freedom of movement for the carboxyl group of the ligand. The double bonded methylene present in PEP can restrict conformations of the ligand. Since methylene is absent in both CEPA and PPA the potential freedom of movement is increased. The third carbon on CEPA could enable more conformations, versus PPA, during a binding event resulting in a reduction of binding affinity.

The individual studies of the bridging oxygen and methylene group were achieved with the use of three additional analogs. Results from PG, methylene minus analog, yield a notable penalty on binding affinity with relatively no change in allosteric coupling. With no other structural difference relative to PEP, results imply a strong role in ligand binding and

little to no role in allosteric coupling for the methylene group. PG analysis also further supports the explanation given above for differences seen in binding between CEPA and PPA. Change to the bridging oxygen is represented in the analog PMAA. When carbon is substituted for the bridging oxygen, as in PMAA, the observable allosteric coupling is all but destroyed and binding affinity is greatly weakened. The lack of allostery seen with PMAA could be a result steric clash due to the bond angle of carbon at the bridging oxygen position combined with the presence of the methylene double bond. The restriction of conformations due to steric conflicts could potentially result in non-preferred ligand conformations. Given the structural similarity to analogs previously mentioned, PMAA does not necessarily clarify the role of the bridging oxygen but rather further supports the importance of methylene to ligand binding.

Given the positioning of MgADP in the binding pocket the results with MgGDP and MgIDP are not surprising. Modifications of the nitrogenous base moiety resulted in minor impacts on binding and virtually no impact on allosteric activity. When MgADP analogs Mg-αβADP results indicate that the electronic and/or physical characteristics are so drastically different from MgADP that no binding is possible.

Like PEP, the necessity of phosphate was determined for MgADP. Two were used to examine the necessity of the presence of phosphate as well as specific need of diphosphate. Adenosine represents the removal of all phosphate, while Mg^{2+} adenosine monophosphate (MgAMP) represents the removal of only one phosphate.

Mutations of residues at position 58 of EcPFK further support the hypothesis of allosteric site interaction with the bridging oxygen. The analysis of PEP with an alanine substitution at position 58 results in a large penalty on both ligand binding and coupling. The

detrimental affect on PEP inhibition by S58A shows similarities to observations with the bridging oxygen analogs. A large affect on both coupling and binding, with a seemingly larger impact on coupling, again suggests the involvement of the of Ser58's hydroxyl group with the bridging oxygen. With a cysteine substitution at the 58 position a notable, but smaller, decrease in ligand affinity observed along with some gain of allosteric coupling, relative to S58A. The relative gain in coupling observed with cysteine could be due to its hydrogen bonding potential of the residue. The potential cysteine as a hydrogen bond donor could also explain S58C's display tighter binding for PEP relative to alanine. We also note that S58C shows a much larger affect on coupling relative to ligand binding. In the case of S58C the 12x increase of Kd, relative to wild type, is still a much higher affinity than what is seen with any of the bridging oxygen analogs in this study.

Mutations at position 58 also display the ability to differentiate between MgADP and PEP. S58A displays a small decrease in ligand affinity for MgADP while having no impact on MgADP coupling. S58C increases the binding affinity for MgADP and has a small decrease in MgADP coupling. The differential treatment between allosteric activator and inhibitor by the EcPFK mutants demonstrates that activation and inhibition are two separate phenomena. While sharing a ligand binding site certainly suggests that the same residues interacting in one allosteric event are used in the other, our data shows the ability of the enzyme to reassign roles in response to an effector ligands identity.

The mechanism by which EcPFK differentiates between PEP and MgADP as inhibitor and activator, respectively, remains unresolved. Previous data, along with the recently solved PEP bound EcPFK crystal structure, have implicated the interaction of effector site residue Ser58, located in α-helix 6, with the oxygen that bridges phosphate to

carbon in PEP. The study of the EcPFK mutant S58A, not only supported the hypothesis of the existence of this interaction but unexpectedly demonstrated the enzyme's ability to differentiate between the two native ligands . Alanine, which served as essentially a hydroxyl deletion, caused the near disappearance of allosteric inhibition along with a 88x increase in PEP dissociation constant. However, with MgADP, S58A had no affect on allosteric coupling and only a 3x increase in dissociation constant. In the study presented here we analyze additional mutations at the serine 58 postion of EcPFK using thermodynamic linkage analysis.

The ability to differentiate between binding and coupling, via thermodynamic linkage analysis, allows for the assignment of roles to ligand functional groups. Use of linkage analysis with effector ligand analogs, limited to minor modifications, allows for role assignment of the methylene and bridging oxygen of PEP. Methylene appears to primarily make contributions to ligand binding. The bridging oxygen makes a large contribution to allosteric coupling while also making a small contribution to ligand binding. Known structural data of EcPFK suggests that serine 58 is a primary residue of interaction for the bridging oxygen. Mutations at this residue position further support the hypothesis of interaction between Ser58 and bridging oxygen. Ser58 also demonstrates the ability to differentiate between allosteric activator and allosteric inhibitor.

REFERENCES

1. PhRMA. (2011) Pharmaceutical Industry Profile 2011, Pharmaceutical Research and Manufacturers of America, Washington DC.
2. Christopoulos, A. (2002) Allosteric binding sites on cell-surface receptors: novel targets for drug discovery, *Nat Rev Drug Discov 1*, 198-210.
3. Cooper, G. M. (2000) *The cell : a molecular approach*, 2nd ed., ASM Press, Sinauer Associates, Washington, D.C., Sunderland, Mass.
4. Alberts, B. (2002) *Molecular biology of the cell*, 4th ed / Bruce Alberts ... [et al.] ed., Garland Science, New York.
5. Jacobson, K. A., Gao, Z. G., Goblyos, A., and Ijzerman, A. P. (2011) Allosteric modulation of purine and pyrimidine receptors, *Adv Pharmacol 61*, 187-220.
6. Koshland, D. E., Jr., Nemethy, G., and Filmer, D. (1966) Comparison of experimental binding data and theoretical models in proteins containing subunits, *Biochemistry 5*, 365-385.
7. Lambert, D. (2004) Drugs and receptors, *Continuing Education in Anaesthesia, Critical Care & Pain 4*, 181-184.
8. Groebe, D. R. (2006) Screening for positive allosteric modulators of biological targets, *Drug Discov Today 11*, 632-639.
9. Bertrand, D., and Gopalakrishnan, M. (2007) Allosteric modulation of nicotinic acetylcholine receptors, *Biochem Pharmacol 74*, 1155-1163.
10. Hogg, R. C., Buisson, B., and Bertrand, D. (2005) Allosteric modulation of ligand-gated ion channels, *Biochem Pharmacol 70*, 1267-1276.

11. Chang, Y., Huang, Y., and Whiteaker, P. (2010) Mechanism of Allosteric Modulation of the Cys-loop Receptors, *Pharmaceuticals 3*, 2592-2609.

12. Conn, P. J., Christopoulos, A., and Lindsley, C. W. (2009) Allosteric modulators of GPCRs: a novel approach for the treatment of CNS disorders, *Nat Rev Drug Discov 8*, 41-54.

13. Ehlert, F. J. (1988) Estimation of the affinities of allosteric ligands using radioligand binding and pharmacological null methods, *Mol Pharmacol 33*, 187-194.

14. De Lean, A., Stadel, J. M., and Lefkowitz, R. J. (1980) A ternary complex model explains the agonist-specific binding properties of the adenylate cyclase-coupled beta-adrenergic receptor, *The Journal of biological chemistry 255*, 7108-7117.

15. Reinhart, G. D. (1988) Linked-function origins of cooperativity in a symmetrical dimer, *Biophys Chem 30*, 159-172.

16. Reinhart, G. D. (2004) Quantitative analysis and interpretation of allosteric behavior, *Methods Enzymol 380*, 187-203.

17. Tlapak-Simmons, V. L., and Reinhart, G. D. (1998) Obfuscation of allosteric structure-function relationships by enthalpy-entropy compensation, *Biophys J 75*, 1010-1015.

18. Johnson, J. L., and Reinhart, G. D. (1994) Influence of MgADP on phosphofructokinase from Escherichia coli. Elucidation of coupling interactions with both substrates, *Biochemistry 33*, 2635-2643.

19. George, S. R., O'Dowd, B. F., and Lee, S. P. (2002) G-protein-coupled receptor oligomerization and its potential for drug discovery, *Nat Rev Drug Discov 1*, 808-820.

20. Gether, U. (2000) Uncovering molecular mechanisms involved in activation of G protein-coupled receptors, *Endocr Rev 21*, 90-113.

21. Vroling, B., Sanders, M., Baakman, C., Borrmann, A., Verhoeven, S., Klomp, J., Oliveira, L., de Vlieg, J., and Vriend, G. (2011) GPCRDB: information system for G protein-coupled receptors, *Nucleic Acids Res 39*, D309-319.

22. Overington, J. P., Al-Lazikani, B., and Hopkins, A. L. (2006) Opinion - How many drug targets are there?, *Nature Reviews Drug Discovery 5*, 993-996.

23. Dorr, P., Westby, M., Dobbs, S., Griffin, P., Irvine, B., Macartney, M., Mori, J., Rickett, G., Smith-Burchnell, C., Napier, C., Webster, R., Armour, D., Price, D., Stammen, B., Wood, A., and Perros, M. (2005) Maraviroc (UK-427,857), a potent, orally bioavailable, and selective small-molecule inhibitor of chemokine receptor CCR5 with broad-spectrum anti-human immunodeficiency virus type 1 activity, *Antimicrobial agents and chemotherapy 49*, 4721-4732.

24. Murdoch, C., and Finn, A. (2000) Chemokine receptors and their role in inflammation and infectious diseases, *Blood 95*, 3032-3043.

25. Insel, P. A., Tang, C. M., Hahntow, I., and Michel, M. C. (2007) Impact of GPCRs in clinical medicine: monogenic diseases, genetic variants and drug targets, *Biochimica et biophysica acta 1768*, 994-1005.

26. Harrington, P. E., and Fotsch, C. (2007) Calcium sensing receptor activators: calcimimetics, *Curr Med Chem 14*, 3027-3034.

27. Davey, A. E., Leach, K., Valant, C., Conigrave, A. D., Sexton, P. M., and Christopoulos, A. (2011) Positive and Negative Allosteric Modulators Promote Biased Signaling at the Calcium-Sensing Receptor, *Endocrinology*.

28. Changeux, J. P., Kasai, M., and Lee, C. Y. (1970) Use of a Snake Venon Toxin to Characterize Cholinergic Receptor Protein, *P Natl Acad Sci USA 67*, 1241-&.

29. Conn, P. M., and Means, A. R. (2000) *Principles of molecular regulation*, Humana, Blackwell Science, Totowa, N.J., Oxford.

30. Thompson, A. J., Lester, H. A., and Lummis, S. C. (2010) The structural basis of function in Cys-loop receptors, *Q Rev Biophys 43*, 449-499.

31. Le Novere, N., and Changeux, J. P. (2001) LGICdb: the ligand-gated ion channel database, *Nucleic Acids Res 29*, 294-295.

32. Alexander, S. P., Mathie, A., and Peters, J. A. (2004) Guide to receptors and channels, 1st edition, *Br J Pharmacol 141 Suppl 1*, S61-70.

33. Lester, H. A., Dibas, M. I., Dahan, D. S., Leite, J. F., and Dougherty, D. A. (2004) Cys-loop receptors: new twists and turns, *Trends Neurosci 27*, 329-336.

34. Morlock, E. V., and Czajkowski, C. (2011) Different residues in the GABAA receptor benzodiazepine binding pocket mediate benzodiazepine efficacy and binding, *Mol Pharmacol 80*, 14-22.

35. Berezhnoy, D., Baur, R., Gonthier, A., Foucaud, B., Goeldner, M., and Sigel, E. (2005) Conformational changes at benzodiazepine binding sites of GABA(A) receptors detected with a novel technique, *J Neurochem 92*, 859-866.

36. Sigel, E., and Buhr, A. (1997) The benzodiazepine binding site of GABAA receptors, *Trends Pharmacol Sci 18*, 425-429.

37. Sine, S. M., and Engel, A. G. (2006) Recent advances in Cys-loop receptor structure and function, *Nature 440*, 448-455.

38. Hunter, T., and Sefton, B. M. (1980) Transforming gene product of Rous sarcoma virus phosphorylates tyrosine, *P Natl Acad Sci USA 77*, 1311-1315.

39. Zhang, X., Gureasko, J., Shen, K., Cole, P. A., and Kuriyan, J. (2006) An allosteric mechanism for activation of the kinase domain of epidermal growth factor receptor, *Cell 125*, 1137-1149.

40. Reed, J. C. (1999) Dysregulation of apoptosis in cancer, *J Clin Oncol 17*, 2941-2953.

41. Blume-Jensen, P., and Hunter, T. (2001) Oncogenic kinase signalling, *Nature 411*, 355-365.

42. Hantschel, O., Grebien, F., and Superti-Furga, G. (2011) Targeting allosteric regulatory modules in oncoproteins: "drugging the undruggable", *Oncotarget 2*, 828-829.

43. Zhang, J., Adrian, F. J., Jahnke, W., Cowan-Jacob, S. W., Li, A. G., Iacob, R. E., Sim, T., Powers, J., Dierks, C., Sun, F., Guo, G. R., Ding, Q., Okram, B., Choi, Y., Wojciechowski, A., Deng, X., Liu, G., Fendrich, G., Strauss, A., Vajpai, N., Grzesiek, S., Tuntland, T., Liu, Y., Bursulaya, B., Azam, M., Manley, P. W., Engen, J. R., Daley, G. Q., Warmuth, M., and Gray, N. S. (2010) Targeting Bcr-Abl by combining allosteric with ATP-binding-site inhibitors, *Nature 463*, 501-506.

44. Daub, H., Specht, K., and Ullrich, A. (2004) Strategies to overcome resistance to targeted protein kinase inhibitors, *Nat Rev Drug Discov 3*, 1001-1010.

45. Schindler, T. (2000) Structural Mechanism for STI-571 Inhibition of Abelson Tyrosine Kinase, *Science 289*, 1938-1942.

46. Nagar, B., Bornmann, W. G., Pellicena, P., Schindler, T., Veach, D. R., Miller, W. T., Clarkson, B., and Kuriyan, J. (2002) Crystal structures of the kinase domain of c-Abl

in complex with the small molecule inhibitors PD173955 and imatinib (STI-571), *Cancer Res 62*, 4236-4243.

47. Faderl, S., Talpaz, M., Estrov, Z., O'Brien, S., Kurzrock, R., and Kantarjian, H. M. (1999) The biology of chronic myeloid leukemia, *N Engl J Med 341*, 164-172.

48. Wood, E. R., Truesdale, A. T., McDonald, O. B., Yuan, D., Hassell, A., Dickerson, S. H., Ellis, B., Pennisi, C., Horne, E., Lackey, K., Alligood, K. J., Rusnak, D. W., Gilmer, T. M., and Shewchuk, L. (2004) A unique structure for epidermal growth factor receptor bound to GW572016 (Lapatinib): relationships among protein conformation, inhibitor off-rate, and receptor activity in tumor cells, *Cancer Res 64*, 6652-6659.

49. May, L. T., Leach, K., Sexton, P. M., and Christopoulos, A. (2007) Allosteric modulation of G protein-coupled receptors, *Annu Rev Pharmacol Toxicol 47*, 1-51.

50. Gao, Z.-G., and Jacobson, K. A. (2006) Keynote review: Allosterism in membrane receptors, *Drug Discov Today 11*, 191-202.

51. PhRMA. (2011) The Research and Development Process, Pharmaceutical Research and Manufacturers of America, Washington DC.

52. Evans, P. R., Farrants, G. W., and Hudson, P. J. (1981) Phosphofructokinase: structure and control, *Philos Trans R Soc Lond B Biol Sci 293*, 53-62.

53. Schirmer, T., and Evans, P. R. (1990) Structural basis of the allosteric behaviour of phosphofructokinase, *Nature 343*, 140-145.

54. Mosser, R., Reddy, M. C., Bruning, J. B., Sacchettini, J. C., and Reinhart, G. D. (2012) Structure of the Apo Form of Bacillus stearothermophilus Phosphofructokinase, *Biochemistry 51*, 769-775.

55. Shirakihara, Y., and Evans, P. R. (1988) Crystal structure of the complex of phosphofructokinase from Escherichia coli with its reaction products, *J Mol Biol 204*, 973-994.

56. Rypniewski, W. R., and Evans, P. R. (1989) Crystal structure of unliganded phosphofructokinase from Escherichia coli, *J Mol Biol 207*, 805-821.

57. Blangy, D., Buc, H., and Monod, J. (1968) Kinetics of the allosteric interactions of phosphofructokinase from Escherichia coli, *J Mol Biol 31*, 13-35.

58. Reinhart, G. D. (1983) The determination of thermodynamic allosteric parameters of an enzyme undergoing steady-state turnover, *Archives of biochemistry and biophysics 224*, 389-401.

59. Monod, J., Wyman, J., and Changeux, J. P. (1965) On the Nature of Allosteric Transitions: A Plausible Model, *J Mol Biol 12*, 88-118.

60. Evans, P. R., Farrants, G. W., and Lawrence, M. C. (1986) Crystallographic structure of allosterically inhibited phosphofructokinase at 7 A resolution, *J Mol Biol 191*, 713-720.

61. Hengartner, H., and Harris, J. I. (1975) Purification by affinity chromatography, properties and crystallisation of phosphofructokinase from thermophilic micro-organisms, *FEBS letters 55*, 282-285.

62. French, B. A., and Chang, S. H. (1987) Nucleotide sequence of the phosphofructokinase gene from Bacillus stearothermophilus and comparison with the homologous Escherichia coli gene, *Gene 54*, 65-71.

63. Berger, S. A., and Evans, P. R. (1991) Steady-State Fluorescence of Escherichia-Coli Phosphofructokinase Reveals a Regulatory Role for Atp, *Biochemistry 30*, 8477-8480.

64. Deville-Bonne, D., Bourgain, F., and Garel, J. R. (1991) pH dependence of the kinetic properties of allosteric phosphofructokinase from Escherichia coli, *Biochemistry 30*, 5750-5754.

65. Berger, S. A., and Evans, P. R. (1992) Site-Directed Mutagenesis Identifies Catalytic Residues in the Active-Site of Escherichia-Coli Phosphofructokinase, *Biochemistry 31*, 9237-9242.

66. Auzat, I., Le Bras, G., Branny, P., De La Torre, F., Theunissen, B., and Garel, J. R. (1994) The role of Glu187 in the regulation of phosphofructokinase by phosphoenolpyruvate, *J Mol Biol 235*, 68-72.

67. Auzat, I., Byrnes, W. M., Garel, J. R., and Chang, S. H. (1995) Role of residue 161 in the allosteric transitions of two bacterial phosphofructokinases, *Biochemistry 34*, 7062-7068.

68. Auzat, I., Le Bras, G., and Garel, J. R. (1997) Allosteric activation increases the maximum velocity of E. coli phosphofructokinase, *J Mol Biol 267*, 476-480.

69. Johnson, J. L., and Reinhart, G. D. (1997) Failure of a two-state model to describe the influence of phospho(enol)pyruvate on phosphofructokinase from Escherichia coli, *Biochemistry 36*, 12814-12822.

70. Kimmel, J. L., and Reinhart, G. D. (2000) Reevaluation of the accepted allosteric mechanism of phosphofructokinase from Bacillus stearothermophilus, *Proc Natl Acad Sci U S A 97*, 3844-3849.

71. Tlapak-Simmons, V. L., and Reinhart, G. D. (1994) Comparison of the inhibition by phospho(enol)pyruvate and phosphoglycolate of phosphofructokinase from B. stearothermophilus, *Arch Biochem Biophys 308*, 226-230.

72. Tie, C., and Reinhart, G. D. (2012) An in vivo approach to isolating allosteric pathways using hybrid multimeric proteins, *Methods Mol Biol 796*, 307-315.

73. Lovingshimer, M. R., Siegele, D., and Reinhart, G. D. (2006) Construction of an inducible, pfkA and pfkB deficient strain of Escherichia coli for the expression and purification of phosphofructokinase from bacterial sources, *Protein Expr Purif 46*, 475-482.

74. Johnson, J. L., and Reinhart, G. D. (1992) MgATP and fructose 6-phosphate interactions with phosphofructokinase from Escherichia coli, *Biochemistry 31*, 11510-11518.

75. Smith, P. K., Krohn, R. I., Hermanson, G. T., Mallia, A. K., Gartner, F. H., Provenzano, M. D., Fujimoto, E. K., Goeke, N. M., Olson, B. J., and Klenk, D. C. (1985) Measurement of protein using bicinchoninic acid, *Analytical biochemistry 150*, 76-85.

76. Kotlarz, D., and Buc, H. (1977) Two Escherichia coli fructose-6-phosphate kinases. Preparative purification, oligomeric structure and immunological studies, *Biochimica et biophysica acta 484*, 35-48.

77. Thaller, C., Weaver, L. H., Eichele, G., Wilson, E., Karlsson, R., and Jansonius, J. N. (1981) Repeated seeding technique for growing large single crystals of proteins, *Journal of molecular biology 147*, 465-469.

78. Otwinowski, Z., Minor, W., and Charles W. Carter, Jr. . (1997) Processing of X-ray diffraction data collected in oscillation mode, *Methods Enzymol. 276*, 307-326.

79. McCoy, A. J. (2007) Solving structures of protein complexes by molecular replacement with Phaser, *Acta crystallographica. Section D, Biological crystallography 63*, 32-41.

80. Winn, M. D., Ballard, C. C., Cowtan, K. D., Dodson, E. J., Emsley, P., Evans, P. R., Keegan, R. M., Krissinel, E. B., Leslie, A. G., McCoy, A., McNicholas, S. J., Murshudov, G. N., Pannu, N. S., Potterton, E. A., Powell, H. R., Read, R. J., Vagin, A., and Wilson, K. S. (2011) Overview of the CCP4 suite and current developments, *Acta crystallographica. Section D, Biological crystallography 67*, 235-242.

81. Adams, P. D., Grosse-Kunstleve, R. W., Hung, L. W., Ioerger, T. R., McCoy, A. J., Moriarty, N. W., Read, R. J., Sacchettini, J. C., Sauter, N. K., and Terwilliger, T. C. (2002) PHENIX: building new software for automated crystallographic structure determination, *Acta crystallographica. Section D, Biological crystallography 58*, 1948-1954.

82. Emsley, P., and Cowtan, K. (2004) Coot: model-building tools for molecular graphics, *Acta crystallographica. Section D, Biological crystallography 60*, 2126-2132.

83. Davis, I. W., Leaver-Fay, A., Chen, V. B., Block, J. N., Kapral, G. J., Wang, X., Murray, L. W., Arendall, W. B., 3rd, Snoeyink, J., Richardson, J. S., and Richardson, D. C. (2007) MolProbity: all-atom contacts and structure validation for proteins and nucleic acids, *Nucleic Acids Res 35*, W375-383.

84. Pettersen, E. F., Goddard, T. D., Huang, C. C., Couch, G. S., Greenblatt, D. M., Meng, E. C., and Ferrin, T. E. (2004) UCSF Chimera--a visualization system for exploratory research and analysis, *J Comput Chem 25*, 1605-1612.

85. Liang, J., Edelsbrunner, H., and Woodward, C. (1998) Anatomy of protein pockets and cavities: measurement of binding site geometry and implications for ligand design, *Protein science : a publication of the Protein Society 7*, 1884-1897.

86. Reinhart, G. D., Hartleip, S. B., and Symcox, M. M. (1989) Role of coupling entropy in establishing the nature and magnitude of allosteric response, *Proc Natl Acad Sci U S A 86*, 4032-4036.

87. Lau, F. T., and Fersht, A. R. (1989) Dissection of the effector-binding site and complementation studies of Escherichia coli phosphofructokinase using site-directed mutagenesis, *Biochemistry 28*, 6841-6847.

88. Pham, A. S., Janiak-Spens, F., and Reinhart, G. D. (2001) Persistent binding of MgADP to the E187A mutant of Escherichia coli phosphofructokinase in the absence of allosteric effects, *Biochemistry 40*, 4140-4149.

89. Pham, A. S., and Reinhart, G. D. (2001) MgATP-dependent activation by phosphoenolpyruvate of the E187A mutant of Escherichia coli phosphofructokinase, *Biochemistry 40*, 4150-4158.

90. Johnson, J. L., and Reinhart, G. D. (1994) Influence of substrates and MgADP on the time-resolved intrinsic fluorescence of phosphofructokinase from Escherichia coli. Correlation of tryptophan dynamics to coupling entropy, *Biochemistry 33*, 2644-2650.

91. Johnson, J. L., Riley-Lovingshimer, M., and Reinhart, G. D. (2004) Unpublished Data.